

Hemispherically asymmetric trade wind changes as signatures of past ITCZ shifts

David McGee^{a,1}, Eduardo Moreno-Chamarro^a, Brian Green^a, John Marshall^a, Eric Galbraith^{b,c},
Louisa Bradtmiller^d

5 ^a Department of Earth, Atmospheric and Planetary Sciences, Massachusetts Institute of
Technology, Cambridge, MA USA; davidmcg@mit.edu; chamarro@mit.edu; brianmg@mit.edu;
jmarsh@mit.edu

^b Institut de Ciència i Tecnologia Ambientals (ICTA) and Department of Mathematics,
Universitat Autònoma de Barcelona, 08193 Barcelona, Spain; eric.d.galbraith@gmail.com

10 ^c ICREA, Pg. Lluís Companys 23, 08010 Barcelona, Spain

^d Department of Environmental Studies, Macalester College, Saint Paul, MN USA;
lbradtmi@macalester.edu

¹Corresponding author: davidmcg@mit.edu

Abstract: The atmospheric Hadley cells, which meet at the Intertropical Convergence Zone (ITCZ), play critical roles in transporting heat, driving ocean circulation and supplying precipitation to the most heavily populated regions of the globe. Paleo-reconstructions can provide concrete evidence of how these major features of the atmospheric circulation can change in response to climate perturbations. While most such reconstructions have focused on ITCZ-related rainfall, here we show that trade wind proxies can document dynamical aspects of meridional ITCZ shifts. Theoretical expectations based on angular momentum constraints and results from freshwater hosing simulations with two different climate models predict that ITCZ shifts due to anomalous cooling of one hemisphere would be accompanied by a strengthening of the Hadley cell and trade winds in the colder hemisphere, with an opposite response in the warmer hemisphere. This expectation of hemispherically asymmetric trade wind changes is confirmed by proxy data of coastal upwelling and windblown dust from the Atlantic basin during Heinrich stadials, showing trade wind strengthening in the Northern Hemisphere and weakening in the Southern Hemisphere subtropics in concert with southward ITCZ shifts. Data from other basins show broadly similar patterns, though improved constraints on past trade wind changes are needed outside the Atlantic Basin. The asymmetric trade wind changes identified here suggest that ITCZ shifts are also marked by intensification of the ocean's wind-driven subtropical cells in the cooler hemisphere and a weakening in the warmer hemisphere, which induces cross-equatorial oceanic heat transport into the colder hemisphere. This response would be expected to prevent extreme meridional ITCZ shifts in response to asymmetric heating or cooling. Understanding trade wind changes and their coupling to cross-equatorial ocean cells is key to better constraining ITCZ shifts and ocean and atmosphere dynamical changes in the past,

especially for regions and time periods for which few paleodata exist, and also improves our understanding of what changes may occur in the future.

Keywords: ITCZ; Hadley circulation; tropics; Heinrich stadials; Quaternary; climate dynamics; global

40

1. Introduction

The paleoclimate record contains abundant evidence of past perturbations of the balance of surface temperatures between the two hemispheres, and as such it provides unique insights into the climate system's response to hemispherically asymmetric heating (Broecker and Putnam, 45 2013; Harrison et al., 1983; Schneider et al., 2014). The clearest examples of such perturbations are millennial-scale coolings of the Northern Hemisphere (stadials) that occurred during the last glacial period (Dansgaard et al., 1982; Alley et al., 1993; Bond et al., 1993; Taylor et al., 1993; Blunier et al., 1998; Blunier and Brook, 2001; EPICA Community Members, 2006; Clement and Peterson, 2008). During these events, expansions of sea ice in the North Atlantic and reduction 50 of cross-equatorial ocean heat transport associated with the Atlantic Meridional Overturning Circulation (AMOC) are thought to have cooled the Northern Hemisphere (NH) (Boyle and Keigwin, 1987; Clement and Peterson, 2008; Henry et al., 2016; Li et al., 2005) and warmed the Southern Hemisphere (SH) (Barker et al., 2009; Blunier et al., 1998; Broecker, 1998; Buizert et al., 2015). The most prolonged of these stadials were also marked by iceberg discharge into the 55 North Atlantic and are known as Heinrich stadials (Hemming, 2004). Stadials have been connected with shifts in the tropical rain belt associated with the Intertropical Convergence Zone (ITCZ) and changes in monsoon strength. A broad range of evidence indicates a southward shift of the ITCZ, a weakening of NH monsoons, and a strengthening of at least the South American

summer monsoon in the SH in response to NH cooling (Arbuszewski et al., 2013; Baker, 2001;
60 Collins et al., 2013; McGee et al., 2014; Peterson, 2000; Placzek et al., 2006; Stager et al., 2011;
Wang et al., 2007, 2004; Wang, 2001).

A variety of modeling experiments have found a qualitatively similar southward shift of
the ITCZ in response to NH cooling. In these studies, ITCZ shifts are accompanied by a
pronounced intensification of the annual-mean Hadley cell in the NH and a weakening in the SH,
65 with each hemisphere's trade winds – the surface expression of the Hadley circulation –
changing in kind (Figures 1 and 2) (Broccoli et al., 2006; Chiang, 2003; Chiang and Bitz, 2005;
Dahl et al., 2005; Timmermann et al., 2005; Vellinga and Wood, 2002; Zhang and Delworth,
2005). As we review below, this asymmetric Hadley cell and trade wind response is a
fundamental expectation of the atmosphere's response to asymmetric cooling of one hemisphere
70 and a shift of the ITCZ toward the warmer hemisphere.

Trade wind changes are central to the dynamics of stadials and other perturbations of
interhemispheric temperature differences. By regulating upwelling along eastern boundaries,
trade winds determine surface productivity and air-sea heat and carbon dioxide fluxes over large
areas of the world's oceans. Trade winds also have a pronounced influence on the ocean
75 circulation, helping drive the circulation of the subtropical gyres and subtropical cells. Attempts
to model ocean circulation in the Atlantic during the Last Glacial Maximum (LGM) have
demonstrated that even small changes in surface trade winds can alter ocean circulation and
improve data-model agreement (Amrhein et al., 2015; Dail and Wunsch, 2014); as such, accurate
characterization of trade wind responses during stadials may be essential to modeling of the
80 ocean's response to these events. Trade winds modulate evaporative fluxes from subtropical
oceans, leading to sea surface temperature (SST) cooling in the hemisphere in which trade winds

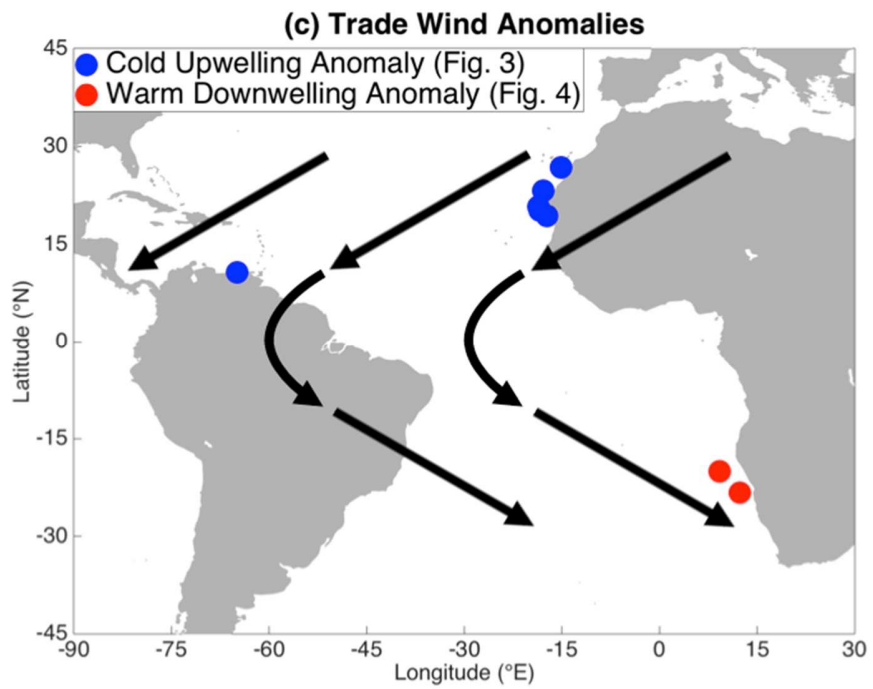
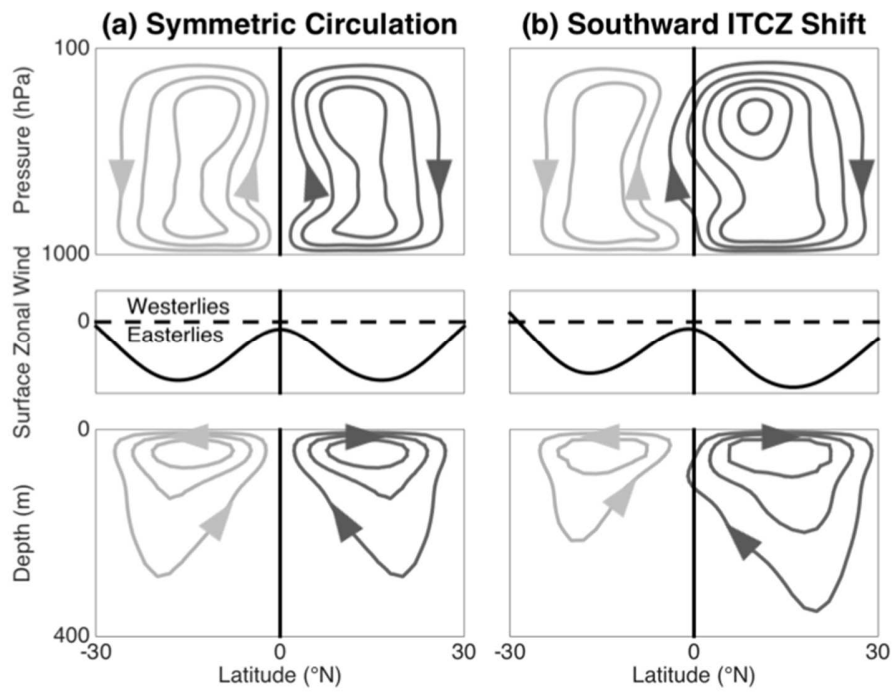
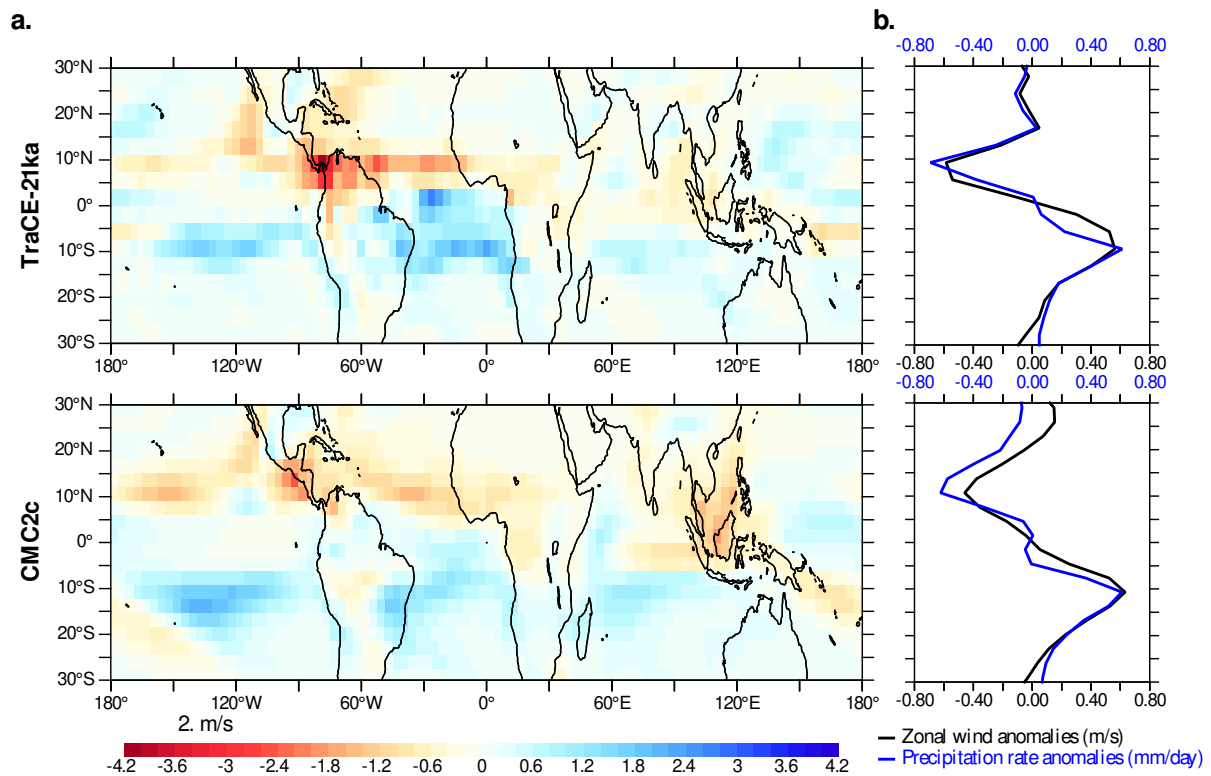


Figure 1. A-B, Idealized zonally averaged Hadley circulation (*top*; with dark grey/light grey describing a clockwise/anticlockwise circulation), surface zonal winds (*center*) between 30°N and 30°S, and zonally averaged subtropical cells (*bottom*, with colors the same as in the top panel) in **(A)** a hemispherically symmetric scenario and **(B)** an asymmetric scenario of a southward ITCZ shift. **C.** Anomalies in surface winds (*arrows*) in response to a southward ITCZ shift. Expected changes in SST and upwelling in response to Heinrich events are shown at sites in the Atlantic Ocean discussed in the text. Panels A and B adapted from Green and Marshall (2017).



95 **Figure 2. A.** Anomalies in annual-mean precipitation rate (in mm/day; *blue-red shading*) and near-surface (10 m) wind (in m/s; *arrows*) between Heinrich Stadial 1 and the LGM (averaged over the periods 16.5-15.5 ka and 21-20 ka respectively) in the TraCE-21ka simulation (*top*) and between the hosing and their respective control experiments with the CM2Mc model (*bottom*). For the latter case the average of the anomalies of the four experiments is shown. **B.** Anomalies, 100 calculated as in **A**, of the zonally averaged, annual-mean precipitation rate (in mm/day; *blue line*) and near-surface zonal wind (in m/s; *black line*) in the TraCE-21ka simulation (*top*) and on average for the CM2Mc experiments (*bottom*).

intensify; this wind-evaporation-SST feedback may play a central role in communicating high-
105 latitude cooling to the low latitudes (Chiang and Bitz, 2005), and may warm tropical SSTs in the
opposite hemisphere, where trade winds are expected to weaken. Perhaps most importantly for
the dynamics of abrupt climate change, trade wind-driven changes in the ocean's subtropical
cells may increase ocean heat transport into the cooler hemisphere, limiting the magnitude of
ITCZ shifts (Green and Marshall, 2017; Yang et al., 2017, 2013).

110 It is thus clear that trade winds are more than passive tracers of atmospheric circulation
changes during NH cooling events; rather, they actively modulate the atmosphere-ocean
system's response to asymmetric warming/cooling. Reconstructions of trade wind changes
during NH cooling events thus have the potential to provide unique insights into the dynamics of
the atmosphere and ocean's response to asymmetric warming or cooling. Proxy-based constraints
115 on trade wind changes are particularly valuable in light of models' long-standing biases in
simulating the ITCZ (Oueslati and Bellon, 2015), which raise questions about the accuracy of
simulated responses to forcing.

Despite this potential, few studies have focused on reconstructing trade wind responses to
changes in the balance of heating between the hemispheres. Most observational studies of the
120 tropical atmosphere's response to NH cooling events have employed precipitation proxies
(Arbuszewski et al., 2013; Baker, 2001; Collins et al., 2013; Peterson, 2000; Sachs et al., 2009;
Schneider et al., 2014; Wang et al., 2004) and have focused on the behavior of the tropical rain
belt and monsoons, leaving changes in the broader Hadley circulation relatively unexplored.
Previous investigations of trade winds in Late Pleistocene climates have primarily focused on
125 single regions and on glacial-interglacial changes. Studies in the eastern subtropical Atlantic
(Sarnthein et al., 1981), the southeastern Atlantic Ocean (Little et al., 1997; Stuut et al., 2002),

the southeastern Indian Ocean (Stuut et al., 2014), and the southeastern Pacific Ocean (Saukel, 2011) have concluded that trade winds in each of these regions were more intense during the last glacial period than today, with little indication of hemispheric asymmetry. A study of past changes in thermocline depth in the western tropical Pacific, which reflects the surface wind field, found evidence for an anomalous thermocline ridge centered at $\sim 6\text{-}7^\circ\text{S}$ during the LGM, consistent either with a southward shift of the ITCZ or a more zonal orientation of the South Pacific Convergence Zone (Leech et al., 2013).

Here we present a compilation of trade wind proxies during Heinrich stadials, the longest and largest-amplitude NH cooling events of the last glacial period and deglaciation, and explore the implications of trade wind changes for the dynamics of these events. This compilation offers an important complement to existing precipitation-based reconstructions, as precipitation proxies are not available everywhere and are particularly sparse over oceans, which underlie the majority of the tropical rain belt. Further, interpretation of precipitation proxies is not always straightforward; each proxy is sensitive to multiple variables, including precipitation amount, evapotranspiration, water vapor source, and convective processes, and the relationship between these variables and the broader Hadley circulation can sometimes be unclear. Trade wind-sensitive proxy data provide additional leverage in testing interpretations of past atmospheric changes, as they directly reflect the tropical atmospheric circulation.

We begin, in Section 2, with a description of the dynamics and observations of the trade winds and their response to Northern Hemisphere cooling in models. In Section 3, we summarize and evaluate proxies for trade wind intensity. In Section 4, we review evidence for trade wind changes associated with Heinrich stadials. We discuss the implications of these results in Section 5, including the role trade winds play in damping the ITCZ response to interhemispheric

150 temperature differences, and close with a summary of key findings and a discussion of directions
for future research in Section 6.

2. Dynamics of wind responses to ITCZ shifts

2.1. Dynamics of the Hadley circulation and trade wind changes accompanying ITCZ shifts

155 Before describing the paleoclimate evidence, we introduce the physical mechanisms
underlying the response of the tropical atmospheric circulation and trade winds to an
interhemispheric heating contrast, as reconstructed during stadials. We start by considering an
idealized state without any heating contrast between the Northern and Southern hemispheres, and
without cross-equatorial energy transport. In this idealized configuration, the zonally averaged
160 tropical atmospheric circulation is symmetric about the Equator in the annual mean; the Hadley
cells and the surface zonal winds are of equal strength in both hemispheres (Fig. 1A). The
ascending branch of the Hadley circulation and the ITCZ are therefore situated at the Equator.

We impose on this symmetric state an interhemispheric heating contrast, with cooling
and warming in the NH and SH extratropics respectively. Such an imbalance is meant to mimic
165 the anomalous heating contrast associated with a shutdown of the AMOC's northward oceanic
heat transport during a Heinrich stadial (e.g., Zhang and Delworth, 2005). Assuming that this
north-south heating contrast is not fully compensated by radiation to space or storage in the
ocean, the atmosphere responds by transporting energy across the Equator to maintain its energy
balance (e.g., Kang et al., 2008). The Hadley cells transport energy in the direction of the air
170 flow within their upper branches, as there is greater moist static energy (the sum of sensible and
latent heat and gravitational potential energy) in their upper branches than in their lower
branches (Neelin and Held, 1987). As a result, a net northward cross-equatorial energy transport
will require an anomalous northward upper-branch flow across the Equator. This is achieved by

shifting the Hadley cells and hence the ITCZ southward, as shown in Fig. 1B. Note that in Fig.
175 1B we also indicate that, along with the southward shift of the system, the NH Hadley cell and
associated trade winds intensify, while the SH Hadley cell and trade winds weaken.

Hemispherically asymmetric changes in the trade winds can be understood to be a
consequence of the (quasi) conservation of angular momentum. Imagine a ring of air encircling
the globe near the Earth's surface along a latitude circle. The rotation of the Earth moves this
180 ring in an eastward direction, termed a 'westerly' velocity. Poleward displacement of that ring
reduces its distance to Earth's axis of rotation, reducing its rotational inertia; if it is to conserve
its angular momentum, it must acquire greater westerly velocity. Applying this concept to a
southward shift of the ITCZ and associated trade winds, a near-surface ring of air in the SH that
shifts poleward away from the Equator will contract toward Earth's axis of rotation and acquire a
185 westerly velocity. Conversely, a southward-shifted ring in the NH expands away from the axis of
rotation and acquires easterly velocity. We therefore expect the trade winds to intensify in the
NH and weaken in the SH, as sketched in Figure 1B. However, the rings' angular momentum is
not perfectly conserved, due to surface friction. The resulting ageostrophic surface wind anomaly
is to the left (right) of the zonal wind anomaly in the NH (SH). This results in a southward
190 (northward) surface trade wind anomaly that strengthens (weakens) the Hadley cell in the NH
(SH), as can be seen comparing Figure 1B to 1A.

A horseshoe pattern of trade wind anomalies emerges when their zonal (i.e., east-west)
and meridional (north-south) components are combined, as shown schematically for a southward
ITCZ shift in the tropical Atlantic in Figure 1C. These drive anomalous Ekman transports in the
195 surface ocean at right angles to the wind – to the right in the NH and to the left in the SH –
which, when combined with the orientation of the coasts, result in enhanced offshore transport at

sites in the NH (blue dots) and reduced offshore transport at sites in the SH (red dots). Enhanced offshore transport at NH sites upwells more cool water from depth and SSTs there are reduced, while reduced offshore transport and upwelling leading to increased SSTs at sites in the SH.

200 Nutrient transport to the photic zone similarly increases in NH upwelling zones and decreases in SH upwelling zones, driving changes in productivity. Strengthened trade winds are also expected to increase windblown mineral dust emissions from subtropical dust sources in the NH, while dust emissions and dust grain size may decrease in the SH subtropics. The physics linking changes in the trade winds, coastal upwelling, SSTs and mineral dust fluxes to ITCZ shifts

205 motivates the study of multiple climate variables when investigating past ITCZ shifts, instead of focusing on changes in precipitation alone.

2.2. Simulated changes in trade winds during ITCZ southward shifts

Modeling studies of anomalous NH extratropical cooling consistently show southward

210 ITCZ shifts and accompanying changes in the trade winds. Climate models forced with cooling in the North Atlantic – by imposing a surface freshwater flux there that shuts down the AMOC’s northward oceanic heat transport, for example – show an anomalous atmospheric energy transport northward across the Equator and a southward ITCZ shift (see the review by Chiang and Friedman, 2012). Intensified NH trade winds and abated SH trade winds, accompanied by

215 anomalous northerlies at the Equator (similar to Fig. 1C), are most clearly seen in the tropical Atlantic Ocean in these simulations (Chiang, 2003; Timmermann et al., 2005; Vellinga and Wood, 2002). Although the same pattern of wind anomalies is not necessarily seen in the other ocean basins (Timmermann et al., 2005; Vellinga and Wood, 2002), zonally averaged wind anomalies clearly reflect those in the tropical Atlantic.

220 We complement these previous modeling studies by exploring results from two different
climate model simulations of Heinrich stadials. Both simulations are made with full-complexity
general circulation models, run at roughly 3-degree resolution for the ocean and atmosphere. The
first is the TraCE-21ka simulation, a transient climate simulation of the last 21,000 years from
the LGM to the present (Liu et al., 2009). It uses the coupled atmosphere–ocean general
225 circulation model CCSM3, and it is forced with changes in the Earth’s orbit, atmospheric CO₂
concentration, ice sheets, sea level, and, during events like Heinrich Stadial 1 or the Younger
Dryas, geologically-informed surface freshwater fluxes via river drainages into the North
Atlantic. The second model ‘simulation’ is actually the average of four different sets of
freshwater hosing experiments performed with the coupled Earth system model CM2Mc, in
230 which the atmospheric CO₂ concentration is set to 180 ppm, and the land-based ice sheet
topography and land cover type of the Paleoclimate Model Intercomparison Project 3 (PMIP3)
LGM state are prescribed (Brown and Galbraith, 2016). The high-latitude land-sea mask and
ocean bathymetry were also adjusted to close the Bering Strait and to eliminate ocean grid cells
beneath ice sheets, but no attempt was made to represent other changes in sea level, given that
235 such changes might introduce unrealistic features considering the coarse resolution of the model.
The CM2Mc experiments are run in four different orbital configurations, reflecting opposite
phases of precession and the maximum and minimum values of obliquity during the Pleistocene.
The orbit’s eccentricity is held constant at 0.03. Each orbital configuration includes a control and
a hosed simulation, in which a 0.2 Sv freshwater input is applied uniformly over a rectangular
240 area in the open North Atlantic Ocean for 1000 years. The mean state for each simulation is
obtained by averaging the final 100-year-long period of the 1000-year hosing interval. In all
cases we show the average of the four orbital configurations as a general response to hosing.

We focus on changes in the climate between Heinrich Stadial 1 and the LGM in the TraCE-21ka simulation, and between the hosing experiments and their respective control runs in the CM2Mc model (Fig. 2). These two cases represent a similar scenario in which a shutdown of the AMOC's northward heat transport induces an anomalous NH cooling. In response to this cooling, and in agreement with the idealized case discussed in Section 2.1, both models exhibit a southward ITCZ shift that reduces tropical rainfall in the NH and increases tropical rainfall in the SH. In the TraCE-21ka simulation, changes in the precipitation rate are most pronounced in the tropical Atlantic, whereas in the CM2Mc experiments the changes are of similar magnitude across most of the tropical region. Both models thus exhibit a global reorganization of tropical precipitation, even though the forcing is confined to the Atlantic Ocean. The change in the zonally averaged precipitation rate is strikingly consistent between the models, and reflects a southward migration in the ITCZ's centroid position (defined following Donohoe et al., 2013) of about 1.2° in the TraCE-21ka simulation, and of about 1.8° on average for the CM2Mc experiments. Given that these are different models, integrated under significantly different forcings, this agreement is remarkable. As shown by Brown and Galbraith (2016), the response of precipitation in CM2Mc to hosing is also quite similar under an interglacial background state, and is even remarkably similar for unforced internal AMOC oscillations. Drier and wetter conditions develop in the NH and SH tropics respectively, with maximum changes in the zonal mean precipitation rate around 10°N and 10°S in both models.

Changes in the trade winds are also robust across the simulations, with an overall intensification in the NH and a weakening in the SH (Fig. 2). Regionally, trade wind anomalies in both models include weakening on the eastern side of all ocean basins in the SH and an intensification in the northern tropical Pacific. In the tropical North Atlantic, by contrast, changes

in the trades differ slightly between the two models: whereas the CM2Mc experiments show a rather continuous belt of intensified coastal trades along the western African coast, the TraCE-21ka simulation exhibits a more complex pattern, with anomalous easterlies and westerlies converging over the eastern tropical North Atlantic and leading to anomalous southerlies along the African coast north of 15°N. Despite these regional differences, a hemispherically asymmetric response of the trade winds associated with a southward ITCZ shift appears as a robust feature in both models (right panels of Fig. 2), and is consistent with the mechanisms described in Section 2.1.

2.3 Response of low-latitude ocean circulation to trade wind changes

The low-latitude ocean circulation is primarily driven by the trade winds. Zonal wind stress from the trade winds drives poleward Ekman transport of shallow tropical waters in both hemispheres; these water masses converge and subduct in the subtropics at approximately 30° latitude. Subducted water flows equatorward in the thermocline at ~300-400 m depth, upwelling at the equator to close the meridionally-overturning subtropical cells (STCs) (Figure 1A, bottom panel) (McCreary and Lu, 1994). Water in the upper limb of the STCs loses heat to the atmosphere as it moves poleward and sinks, leading to a strong temperature gradient between the upper and lower limbs of the STCs. As a result, the STCs are the ocean's primary means of transporting heat from the tropics to the subtropics and closely mirror the atmosphere's Hadley cells (Held, 2001; Klinger and Marotzke, 2000; Trenberth and Caron, 2001).

The direct relationships between the Hadley cells, trade winds, and STC strength in each hemisphere imply that hemispherically asymmetric trade wind changes accompanying Hadley cell shifts will drive similarly asymmetric changes in STC strength. As shown by Green and

Marshall (2017), this response results in cross-equatorial flow of warm surface waters into the
290 cooler hemisphere due to relative strengthening of the cooler hemisphere's trade winds and
STCs. The anomalous cross-equatorial STC circulation thus transports heat into the cooler
hemisphere, partially offsetting the inter-hemispheric heating contrast and damping the
atmosphere's response. We explore the implications of this point for ITCZ shifts in Section 5.

295 **3. Trade wind proxies**

Changes in past trade wind intensity are most often reconstructed using marine sediment
records of upwelling and windblown dust. Dust fluxes respond sensitively to changes in surface
wind speed, as dust emissions increase at a factor of roughly the cube of the wind speed once a
threshold speed is reached (Gillette, 1974; McGee et al., 2010). Dust grain size (either the modal
300 size or the proportion of grains greater than a given size) is expected to increase with increased
wind speed (Rea, 1994; Stuut et al., 2002). Sand dune activity is also strongly influenced by
wind speed (Roskin et al., 2011; Tsoar, 2005), so reconstructions of dune field activity in trade
wind regions can also provide insight into past wind intensity.

However, dust fluxes, grain size and dune activity are each subject to additional controls
305 beyond mean wind speed. Dust flux and dune activity can vary with source aridity, and both flux
and grain size are expected to increase if the distance to the source decreases, for example due to
exposure of continental shelves in response to falling sea level. The grain size of dust deposited
at downwind sites can also change due to changes in dust source area properties (such as the
proportion of coarse grains) (Grini and Zender, 2004), changes in the balance of dry deposition
310 (settling) vs. deposition by precipitation scavenging, and changes in transporting winds rather
than source area winds. In addition, dust-related proxies reflect dust storms and thus tell us about

a long-term mean of high-wind-speed events rather than directly reflecting mean trade wind speed. Nevertheless, it is likely that strong wind events increase with mean trade wind speed, based on the common observation that wind speed variance (and thus the occurrence of strong winds) increases with increasing mean wind speed (Grini and Zender, 2004; Wang et al., 2015).

Coastal upwelling also responds sensitively to changes in surface trade winds when the relative orientation of winds and coastlines causes Ekman transport to move surface waters offshore. In this case, which most commonly occurs along eastern boundaries of subtropical oceans, strengthening of trade winds leads to cooler SSTs and an increased supply of nutrients to the photic zone. These nutrients increase primary productivity and alter species distributions in surface waters, and respiration of sinking organic matter causes dissolved oxygen levels to drop in intermediate-depth waters. As a result, records of the accumulation rate of biogenic sediments (e.g., organic carbon, biogenic opal), species distributions, SSTs and the oxygenation of intermediate-depth bottom waters in upwelling zones have been interpreted to reflect past changes in upwelling intensity (that is, vertical velocities in upwelling zones).

However, each of these indicators is controlled by additional factors beyond trade wind speed. Changes in biogenic sediment flux may also reflect changes in the nutrient content of upwelled water (Takesue et al., 2004) or in preservation efficiency in sediments rather than upwelling intensity. Changes in SST may result from changes in the temperature of upwelled waters or surface-advected waters without changes in upwelling intensity. Species distributions may also change due to changes in the temperature and/or nutrient content of upwelled waters. Subsurface oxygenation can change due to changes in the oxygen content of waters entering the upwelling zone rather than oxygen demand (Schmittner et al., 2007). Upwelling at a given site may also respond to changes in wind stress curl (the spatial gradient of wind speed) in addition

335 to changes in wind speed. The importance of the spatial distribution of the wind stress curl has particularly been noted in the Arabian Sea (Le Mézo et al., 2017), as changes in the position of the wind speed maximum can lead to opposite nearshore and offshore responses.

The multiple controls on each potential trade wind proxy suggest that we must be cautious in inferring past changes in trade winds and must evaluate the potential for other factors to produce the observed signals. In this study, we focus on regions for which responses during Heinrich stadials are recorded by multiple proxy types, as many of these proxies are reasonably independent of each other (e.g. dust grain size vs. SSTs), and paired changes in records from the same region are best explained by changes in winds. Where multiple proxy types are not available, we evaluate the likelihood that the observed changes are the result of variations in trade wind speed.

The trade wind proxies described above are interpreted qualitatively, as indicating either increases or decreases in wind strength but not the magnitude of these changes. Sea surface and subsurface temperature proxies can be compared directly between models and data to test whether simulated wind changes are approximately similar to the changes reflected in proxy records, as long as the seasonality and depth recorded by temperature proxies is understood (e.g., Tierney et al., 2015). Quantitative data-model comparisons are also possible for other proxies through the use of forward models simulating proxy responses from model output ("proxy system models"; Evans et al., 2013; Goose, 2016). Initial efforts have been made to model the productivity and dust responses during Heinrich stadials and to compare simulated changes to proxy data (Albani et al., 2016; Mariotti et al., 2012; Murphy et al., 2014). Further work building on these studies may allow us to place quantitative bounds on past trade wind changes and to better test data-model agreement.

4. Trade wind changes and ITCZ shifts in paleoclimate records

360 We now review evidence for changes in trade wind intensities during Heinrich stadials,
which exhibit the largest perturbations to the balance of surface heating between the hemispheres
(Figure 3A) and the clearest examples of shifts of the annual-mean ITCZ in the recent paleo-
record (Clement and Peterson, 2008; McGee et al., 2014; Schneider et al., 2014). We focus in
particular on the most recent two stadials – Heinrich Stadial 1 (~18-15 ka) and the Younger
365 Dryas (12.9-11.7 ka) – because of the increased data availability and data quality for these
intervals, but we also examine previous Heinrich stadials when possible. We assess the
robustness of proxy evidence for changes in the trade winds and then look for regional and
interhemispheric differences in trade wind responses to build a clearer picture of atmospheric
circulation changes during these periods. Sediment core locations and a summary of observations
370 from each core are included in Table 1.

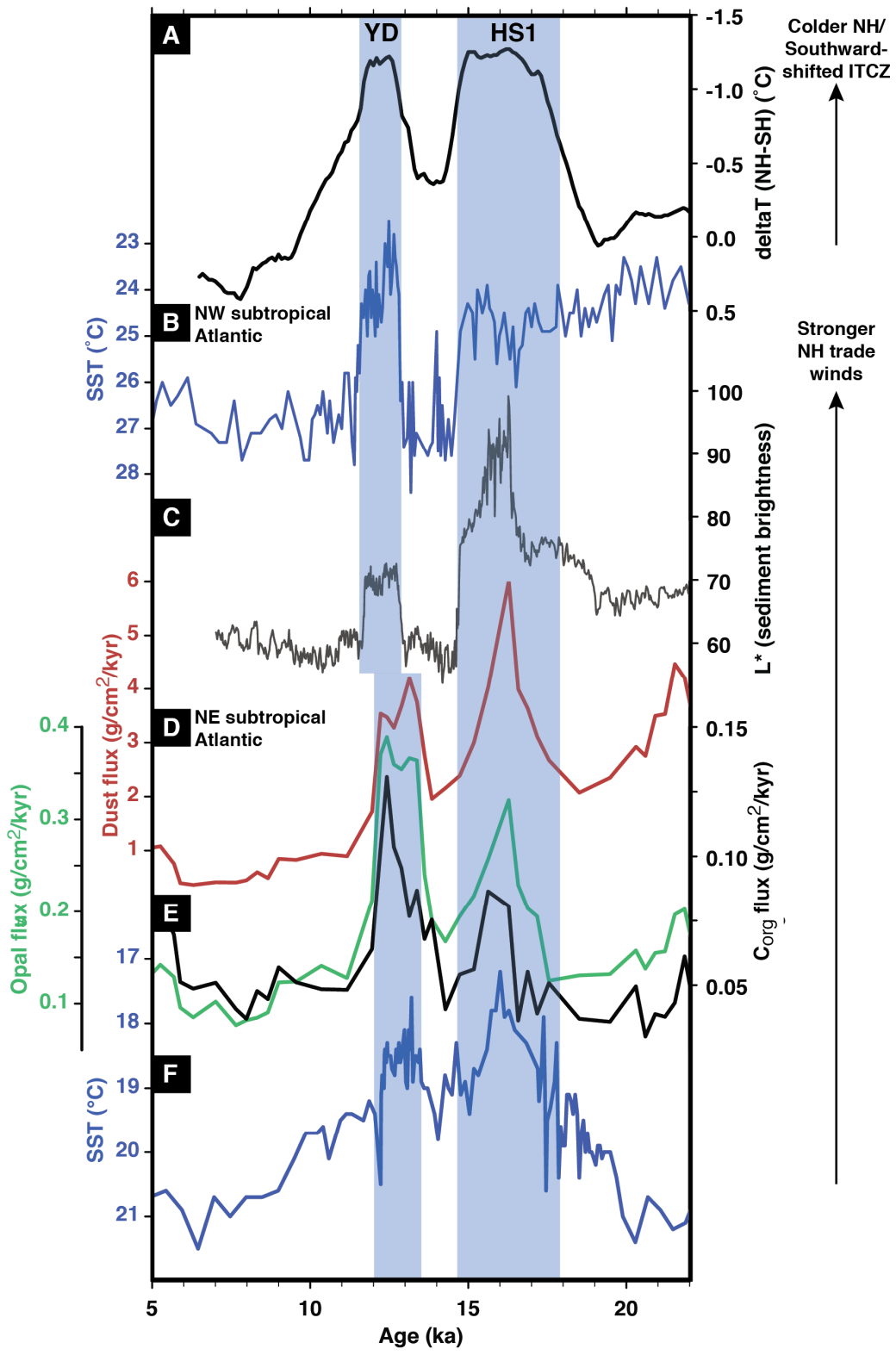
4.1 Northern Hemisphere trade winds during Heinrich stadials

4.1.1 North Atlantic

The clearest trade wind signals during Heinrich stadials are in the subtropical North
375 Atlantic. Along the northwest African margin, a variety of marine sediment records document
increases in windblown dust flux or dust abundance during Heinrich stadials (Figure 3D)
(Adkins et al., 2006; Collins et al., 2013; McGee et al., 2013; Tjallingii et al., 2008). Records of
biogenic sediment composition and flux from the NW African margin also document increases
in opal and organic carbon accumulation during Heinrich stadials (Figure 3E) (Bradt Miller et al.,
380 2016; Romero et al., 2008). In addition, SST reconstructions from the region indicate SST

minima during Heinrich stadials (Figure 3F) (Romero et al., 2008). Though each of these records in isolation could reflect other environmental factors, the dust, productivity and SST records together paint a consistent picture of substantially intensified trade winds along the NW African margin during Heinrich stadials (BradtMiller et al., 2016; Romero et al., 2008), with the best data availability for HS1 and the YD. Based on the modern seasonality of coastal upwelling and dust transport in this region, it is most likely that these changes reflect increases in winter trade winds (Anderson et al., 2016; Bradtmiller et al., 2016; McGee et al., 2013).

On the other side of the subtropical North Atlantic, easterly trade winds associated with the southward shift of the ITCZ during boreal winter drive upwelling in the Cariaco Basin off the northern coast of Venezuela, as Ekman transport moves waters offshore (Peterson et al., 1991). High-resolution records from the Cariaco Basin show evidence for SST cooling during the Younger Dryas and, to a lesser extent, during Heinrich Stadial 1 (Figure 3B) (Lea, 2003). The Younger Dryas and the end of Heinrich Stadial 1 are also marked by lighter sediment color, taken to represent increased surface productivity (Figure 3C) (Deplazes et al., 2013; Hughen et al., 1996), and increased abundance of upwelling-adapted species (*G. bulloides* and diatoms) (Dahl et al., 2004; Peterson et al., 1991). Longer records suggest that similar changes in sediment color accompany stadials throughout the last glacial cycle (Deplazes et al., 2013). Together, these findings point to increased trade wind-driven upwelling in the western subtropical North Atlantic during Heinrich stadials, suggesting trade wind intensification across the breadth of the low-latitude North Atlantic. When compared with the modeling results shown in Fig. 2, we find the best model–data agreement with the CM2Mc model, where a clear pattern of intensified trade winds is simulated in the tropical North Atlantic.



405 **Figure 3.** Examples of trade wind proxies from the North Atlantic showing evidence for NH
trade wind intensification in association with implied southward ITCZ shifts during Heinrich
Stadial 1 (HS1) and the Younger Dryas (YD). **A.** Reconstruction of hemispheric surface
temperature difference (Shakun et al., 2012); **B.** Mg/Ca-based SST reconstruction from Cariaco
Basin core PL07-39PC (Lea, 2003); **C.** Sediment color from Cariaco basin core MD03-2621,
410 with higher values interpreted as reflecting higher primary productivity (Deplazes et al., 2013);
D. Dust flux reconstruction from NW African margin core OCE437-7 GC68 (McGee et al.,
2013); **E.** Reconstructions of opal and organic carbon fluxes from NW African margin core
OCE437-7 GC68 (Bradtmitter et al., 2016); **F.** Alkenone-based SST data from NW African
margin core Geob7926-2 (Romero et al., 2008). The offset in the age of the YD in the African
415 margin cores may reflect changes in surface water radiocarbon age in this region. Note flipped
vertical axis directions on temperature plots. Core locations listed in Table 1.

4.1.2 Arabian Sea

In the Arabian Sea, southwesterly winds associated with the Indian summer monsoon
420 drive upwelling and high productivity along the Oman and Somali margins during the summer
months, and northeasterly winter winds reduce upwelling due to the orientation of the coastlines.
A variety of proxy records of upwelling intensity and subsurface temperatures are consistent
with a reduction in upwelling during Heinrich stadials throughout the last glacial period. These
records indicate reduced total organic carbon (TOC) content in sediments (Figure 4A)
425 (Ivanochko et al., 2005; Schulz et al., 1998); nitrogen isotope data suggesting reduced water
column denitrification, interpreted as reflecting reduced oxygen demand from sinking organic
matter (Figure 4B) (Altabet et al., 2002; Ivanochko et al., 2005); and increased subsurface
temperatures, consistent with reduced vertical mixing and heat loss to the atmosphere during
winter (Figure 4C) (Huguet et al., 2006; Tierney et al., 2015). Dust fluxes in the Arabian Sea also
430 increase substantially during several Heinrich stadials (Figure 4D) (Pourmand et al., 2004),
suggesting an increase in northerly winter winds transporting dust from the Arabian peninsula
and South Asia. As seen in Figure 4, the Heinrich stadials are best captured by the high-
resolution TOC and nitrogen isotope records, but the lower resolution subsurface temperature
and dust flux records also show consistent changes during HS1 and the YD.

435 Proxy data are thus consistent with a reduction in southwesterly summer monsoon winds
and an intensification of northeasterly winter trade winds in the Arabian Sea during Heinrich
stadials. Though this seasonal wind reversal characterizes the South Asian monsoon system, the
winds project strongly onto the zonal mean Hadley circulation and constitute a major portion of
interhemispheric atmospheric heat transport associated with the annual mean, zonal mean
440 tropical circulation (Heaviside and Czaja, 2013). Regardless of the seasonal balance of wind

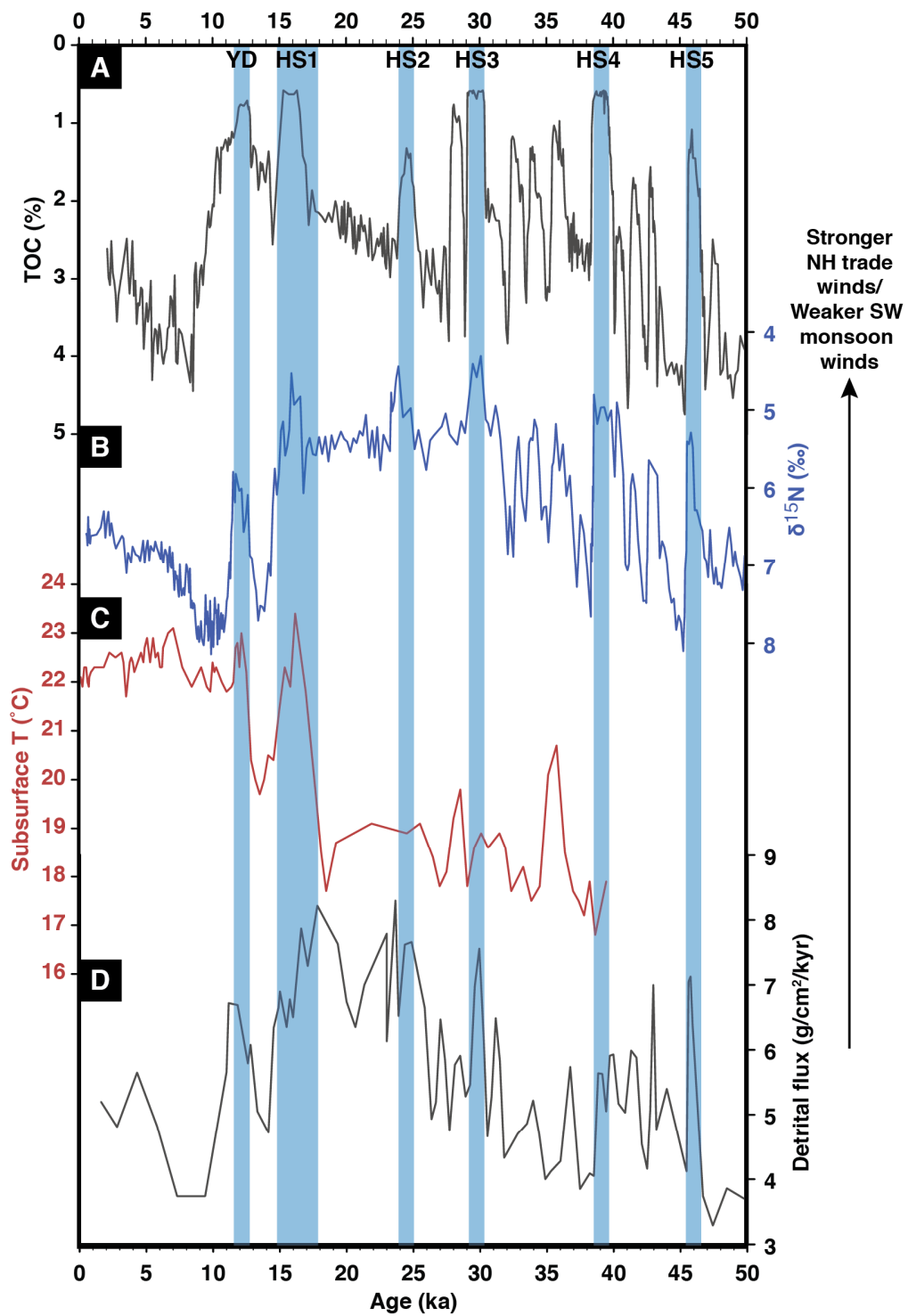


Figure 4. Wind proxies from the Arabian Sea showing evidence for northeasterly trade wind

intensification and southwesterly monsoon wind weakening in association with implied southward ITCZ shifts during Heinrich Stadials (HS) and the Younger Dryas (YD). **A.** Total organic carbon (TOC) content of core SO90-136KL (Schulz et al., 1998), on reversed axis; **B.** nitrogen isotope data from core NIOP905 (Ivanochko et al., 2005), on reversed axis; **C.** Subsurface temperature reconstruction from core P178-15P (Tierney et al., 2015); **D.** Dust flux reconstruction from core SO90-93KL (Pourmand et al., 2004). Core locations listed in Table 1.

450

changes, weakening of summer southwesterly winds and strengthening of winter northeasterly winds during stadials produce northeasterly wind anomalies in the annual mean that weaken both the lower branch of the zonally and annually averaged Hadley circulation and the wind-driven oceanic subtropical cell in the NH portion of the Indian Ocean (Section 5). Consistent with these reconstructed changes, the model simulations considered here show northerly and northeasterly wind anomalies in the Arabian Sea in the annual mean (Figure 2a), as well as in both winter (DJF) and summer (JJA; not shown).

460 **4.1.3 North Pacific**

Reconstructing trade wind changes in the tropical and subtropical North Pacific poses a greater challenge. There are no high-resolution dust records reflecting short-range transport, as regional dust sources in the trade wind belt (e.g., the deserts of western Mexico) are weak. Coastal upwelling records are complicated by the fact that most coastlines in the northeast tropical Pacific trend southeast/northwest, orthogonal to canonical trade wind directions. As detailed below, changes in the nutrient content and temperature of upwelled waters also obscure interpretation of upwelling records.

In Baja California, where wind-driven upwelling occurs throughout the year (Takesue et al., 2004), marine sediments document minima in organic carbon accumulation and benthic foraminifera abundance during most Heinrich stadials of the last 50 ka (Cartapanis et al., 2011; Ortiz et al., 2004). Similarly, records from the Gulf of California indicate reduced opal abundance and increasing SSTs during Heinrich stadials of the last 50 ka (Cheshire and Thurow, 2013; McClymont et al., 2012). These indications of reduced surface ocean productivity and increasing SSTs may seem to indicate weakened trade winds during Heinrich stadials. However,

475 Ortiz et al. (2004) suggest that this pattern primarily reflects a shift to El Niño-like conditions in
the tropical Pacific during Heinrich stadials, which would lead to a deepened regional
thermocline/nutricline and thus a reduction in nutrient content and increase in temperature in
upwelled waters. Modern observations of upwelling and nutrients in southern Baja California
indicate that nutrient delivery to the surface can be reduced during and immediately following El
480 Niño events due to deepening of the regional nutricline even in the presence of strengthened
coast-parallel winds and upwelling intensity (Takesue et al., 2004). At present it is unclear
whether Heinrich stadials were characterized by El Niño- or La Niña-like mean states (e.g.,
Prange et al., 2010), or whether ENSO is an inappropriate analogue for regional ocean-
atmosphere changes during stadials (Leduc et al., 2009; McClymont et al., 2012). At the very
485 least, modern data suggest that upwelling records in the subtropical North Pacific may primarily
reflect changes in the equatorial Pacific thermocline rather than local trade wind strength.

Closer to the equator in the North Pacific, records of opal accumulation and diatom
species assemblages at a coastal site off the Costa Rica margin in the Panama Basin indicate
lower nutrient supply and decreased opal flux during Heinrich stadials (Romero et al., 2011).
490 These indicators of decreased upwelling are interpreted by the authors to represent increased
northeasterly winds, as the site lies in the lee of the Central American highlands (Talamanca
Cordillera) and experiences downwelling due to the wind stress curl driven by northeasterly
wind jets traveling through topographic gaps (Romero et al., 2011). The speed of these wind jets
is correlated with regional trade wind strength (Chelton et al., 2000), supporting a connection
495 between overall trade wind strength, wind jet strength, and downwelling intensification at this
core site.

Just north of the equator in the eastern Pacific, Heinrich Stadial 1 and the Younger Dryas are marked by SST minima and maxima in organic carbon and opal accumulation rates (Kienast et al., 2006). These changes are interpreted by the authors to reflect increased northeasterly trades during these periods, consistent with expectations. However, without more data it is not clear whether these responses were caused by changes in northeasterly trade winds, the temperature and nutrient content of upwelled waters, or changes in southeasterly trade winds.

Improved trade wind reconstructions in the Pacific would be valuable for clarifying equatorial Pacific ENSO dynamics and the Pacific ITCZ response during Heinrich stadials. Hosing simulations suggest that the trade wind-driven Pacific STC response to NH cooling plays a major role in increasing heat transport into the NH during stadials (Yang et al., 2017, 2013), and additional proxy data could assist in testing this simulated response. Proxy data are also of particular value in this region because its modern climatology is poorly represented in models, which tend to overestimate rain belt precipitation south of the equator (Oueslati and Bellon, 2015). As a result, model simulations of ITCZ responses to past climate changes in this region may not be accurate.

4.2 Southern Hemisphere trade winds during Heinrich stadials

The highest-quality trade wind-related records in the SH exist in the subtropical South Atlantic near the Benguela upwelling system. Records of windblown dust grain size indicate a rapid reduction in dust grain size off the coast of southwest Africa during HS1, reflecting reduced transport of coarse-grained dust from sources in the Kalahari Desert (Figure 5B) (Stuut et al., 2002). Similar reductions appear to correspond to Heinrich stadials 3 through 5 and possibly HS2 as well, though the age model of this core leaves uncertainty as to the precise

520 timing of these events. As dust grain size is unlikely to respond so coherently to changes in
aridity, and as there is no evidence for changes in distance to dust sources beyond the gradual
impact of glacial-interglacial sea level changes, the authors interpret these changes as reflecting
the strength of dust-generating trade winds. Future work should aim to more precisely test the
correspondence of these grain size changes with Heinrich stadials and develop dust flux records
525 to accompany the grain size data.

Nearby in the northern portion of the Benguela upwelling system, Little et al. (1997) find
reductions in upwelling-sensitive coldwater species (*N. pachyderma*) during Heinrich stadials of
the last 50 ka, including a large reduction during HS4 and a rapid decline at the beginning of
HS1 (Figure 5). The authors interpret this result as reflecting reduced trade wind intensity during
530 Heinrich stadials. Finally, alkenone-based SST records suggest pronounced warming in the
Benguela system during HS1 (Kim et al., 2003, 2002). Taken together, these dust grain size,
faunal abundance and SST data suggest reductions in trade wind strength in the southeast
Atlantic during Heinrich stadials.

Fewer wind-related records are available in other regions of the SH subtropics. In marine
535 sediments from the Peruvian margin, Saukel (2011) documents a rapid reduction in windblown
dust flux early in the deglaciation. This core site primarily receives windblown dust from the
Atacama Desert (Saukel et al., 2011), a region that has been dry for at least the last 2 million
years (Amundson et al., 2012); as a result, dust fluxes are unlikely to be modulated by aridity
changes and are likely to directly reflect changes in surface wind strength, making this an
540 excellent region for dust-based reconstructions of winds. Similarly, a record of dust abundance
from the eastern Indian Ocean off the coast of northwestern Australia suggests steep drops in
dust abundance and grain size during the deglaciation (Stuut et al., 2014). Unfortunately, neither

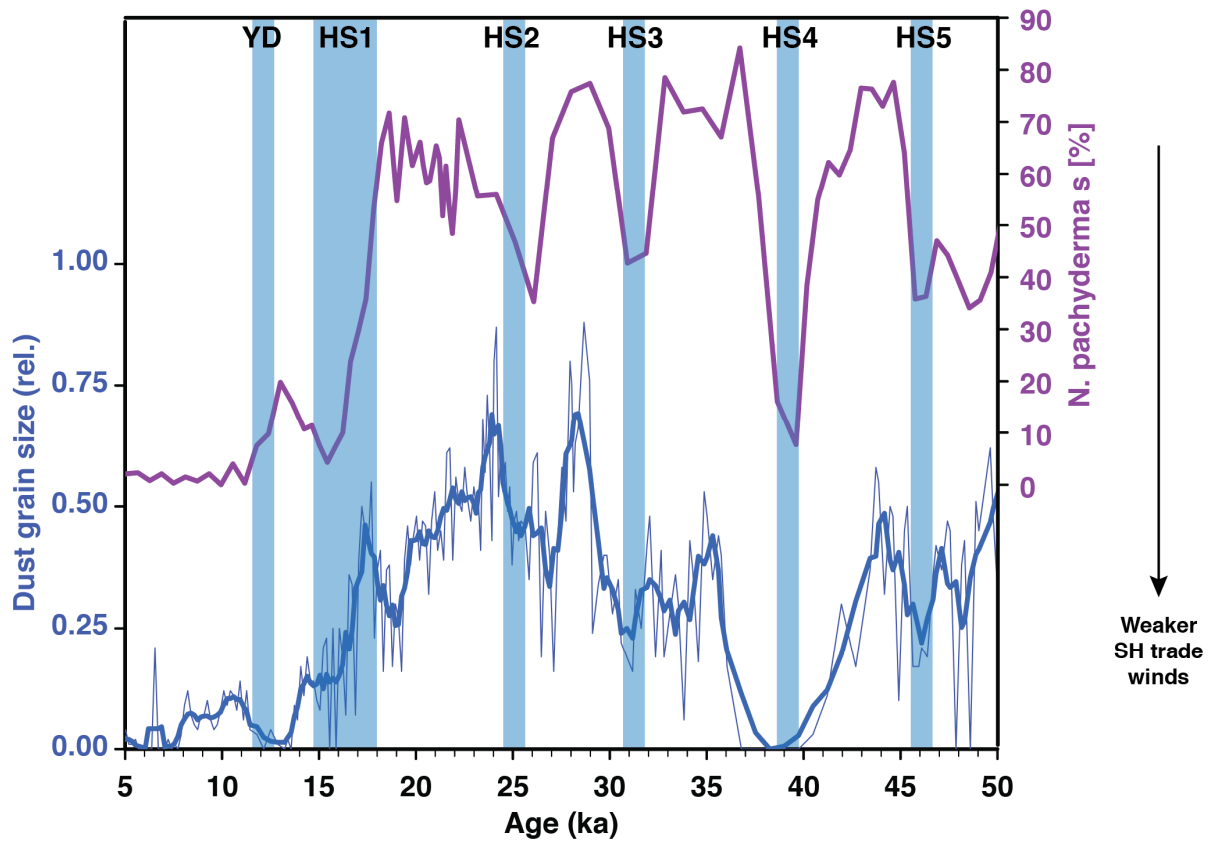


Figure 5. Trade wind proxies from the South Atlantic showing evidence for trade wind

545 weakening in association with southward ITCZ shifts during Heinrich stadials of the last 50 ka.

A. Abundance of *N. pachyderma*, an indicator of reduced SSTs and increased upwelling, in core

GeoB1711-4 (Little et al., 1997). **B.** Dust grain size, expressed as the relative abundance of

coarse-grained dust to total windblown dust, in core MD96-2094 (Stuut et al., 2002). Core

locations listed in Table 1.

550

of these records has the chronological control or temporal resolution necessary to pin down the timing of these deglacial declines in dust flux or to document changes during previous Heinrich stadials, but the steep one-step drops are similar to the changes recorded in the southeast Atlantic during HS1.

555 These dust and upwelling records suggest reductions in trade wind intensity in the South Atlantic during Heinrich stadials. As shown in Figure 2, models suggest a clear pattern of weakened trade winds in all ocean basins of the SH in association with a southward ITCZ shift, but improved records from the South Pacific and South Indian Oceans are needed to test for similar responses in these regions. One puzzle is that SH records do not suggest coherent
560 fluctuations in trade wind strength after HS1 during the Antarctic Cold Reversal/Bølling-Allerød interstadial and Younger Dryas stadial. In part, this may reflect the fact that some proxies used in these records (e.g. dust grain size, dust flux, *N. pachyderma* abundance) become less sensitive in warmer climates that may have overall weaker trade winds and warmer ocean temperatures. However, some records suggest cooling of Benguela region SSTs during the YD, a response
565 opposite to that expected in response to a southward shift of the ITCZ at this time (Farmer et al., 2005; Kim et al., 2003, 2002). Further research is required to better document upwelling and dust changes in the SH during the latter half of the deglaciation.

5. Discussion: Significance of trade wind changes during Heinrich stadials

570 Taken together, these data point to systematic strengthening of NH trade winds and weakening of SH trade winds in the Atlantic basin during Heinrich stadials (Figure 6), with some

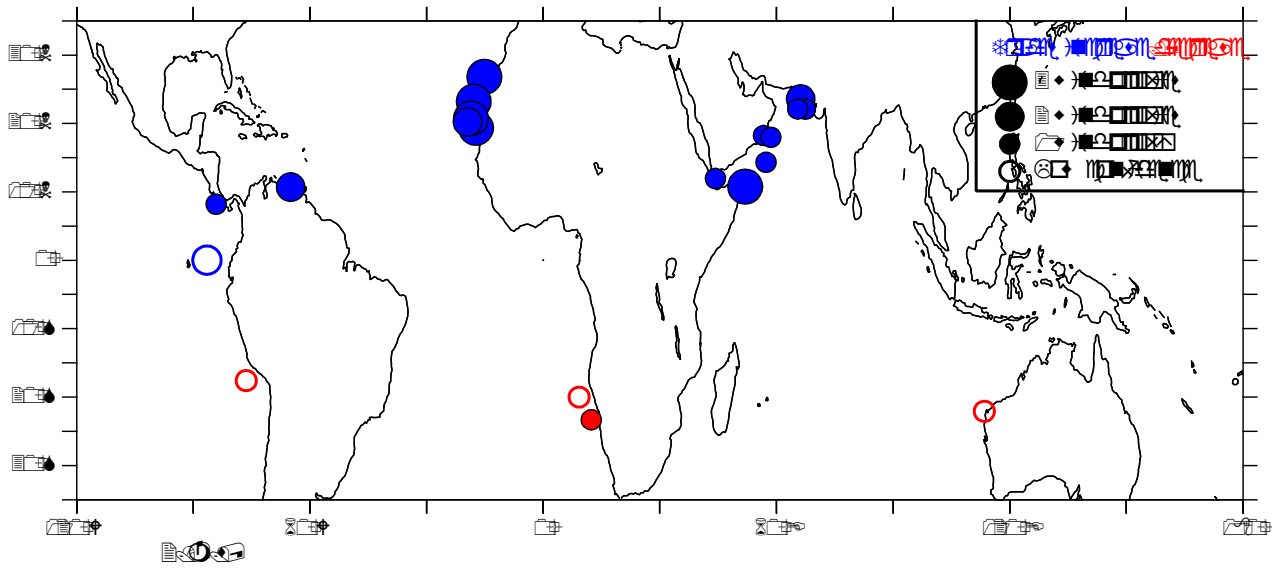


Figure 6. Map of proxy inferences of trade wind changes during Heinrich stadials on top of map
 575 of annually averaged near-surface wind anomalies (10 m) from the CM2Mc hosing experiment,
 from Figure 2A. Blue: implied increase in trade wind strength. Red: implied decrease in trade
 wind strength. Symbol size indicates the number of trade wind proxies (e.g., SSTs, productivity,
 dust flux) available at each site. Empty symbols indicate records with insufficient chronological
 control or temporal resolution or with questions as to their interpretation. Some symbols have
 580 been slightly displaced to make them visible on the map.

indications of similar responses in the Pacific and Indian basins. This asymmetric response is consistent with that predicted in association with a southward ITCZ shift, as the southerly location of the ITCZ is expected to lead to an intensification of the NH Hadley cell and associated trade winds and a weakening of the SH Hadley cell and trade winds (Section 2).

The finding of asymmetric trade wind responses during stadial events in proxy data is significant for several reasons. First, it reinforces reconstructions of southward shifts of the ITCZ during Heinrich stadials based on precipitation proxies (Hodell et al., 2008; Peterson, 2000; Wang et al., 2004) and tropical SST gradients (McGee et al., 2014). This finding thus further strengthens the relationship between asymmetric high-latitude cooling, hemispheric energy budgets, ITCZ location and Hadley cell strengthening/weakening that is central to our understanding of ITCZ position and Hadley cell dynamics (Chiang and Friedman, 2012; Donohoe et al., 2013; Kang et al., 2008; Marshall et al., 2014; Schneider et al., 2014). Asymmetric trade wind responses also suggest that wind-evaporation-SST feedbacks may have played a significant role in communicating high-latitude Northern Hemisphere cooling to the tropical North Atlantic (Chiang and Bitz, 2005).

The trade wind changes reconstructed here may also have played a role in driving the monsoon responses consistently observed during Heinrich stadials. Enhanced North Atlantic boreal winter trade winds are likely to increase moisture advection into northern South America (Garcia and Kayano, 2010; Vuille et al., 2012), leading to strengthening of the South American summer monsoon during Heinrich stadials as observed in proxy data (Baker and Fritz, 2015; Placzek et al., 2006; Strikis et al., 2015; Wang et al., 2017, 2007). Strengthening of NH northeasterly winds also increases the advection of cold, dry air from higher latitudes into NH

monsoon regions; this “ventilation” contributes to monsoon weakening during Heinrich stadials,
605 particularly in North Africa (Liu et al., 2014).

Hemispherically asymmetric trade wind changes are also likely to have altered the strength of the ocean’s overturning STCs, in which waters move from equatorial regions to the subtropics at the surface, then sink and return to low latitudes at thermocline depths (~300-400 m) (Section 2.3). Though these cells are much shallower than the ocean’s deep overturning
610 circulation, they transport a similar magnitude of heat due to the large difference in temperature between the upper and lower limbs (Held, 2001; Klinger and Marotzke, 2000). In response to strengthening of NH trade winds and weakening of SH trade winds, an anomalous shallow cross-equatorial circulation develops that transports surface waters and heat from the SH into the NH (Figure 7A). This increased northward heat transport in the shallow ocean offsets a significant
615 portion (~30-40%) of the ocean heat transport anomaly associated with reductions in AMOC in GCM hosing simulations designed to resemble Heinrich stadials (Yang et al., 2017, 2013). In idealized simulations by Green and Marshall (2017) in which hemispheric energy budgets are perturbed, ITCZ shifts in fully coupled ocean-atmosphere simulations are much smaller than shifts in uncoupled (slab ocean) experiments (Figure 7B). The authors attribute most of this
620 difference to the role of the oceans’ subtropical cells in amplifying the heat transport into the cooler hemisphere associated with an ITCZ shift (Green and Marshall, 2017).

The large changes in cross-equatorial atmospheric heat transport that accompany relatively small (1-2 degrees latitude) changes in zonal mean ITCZ position make it unlikely that the ITCZ has been far from the equator in the past unless heat transports associated with the
625 Hadley circulation were very different (Donohoe et al., 2013; McGee et al., 2014). The STC

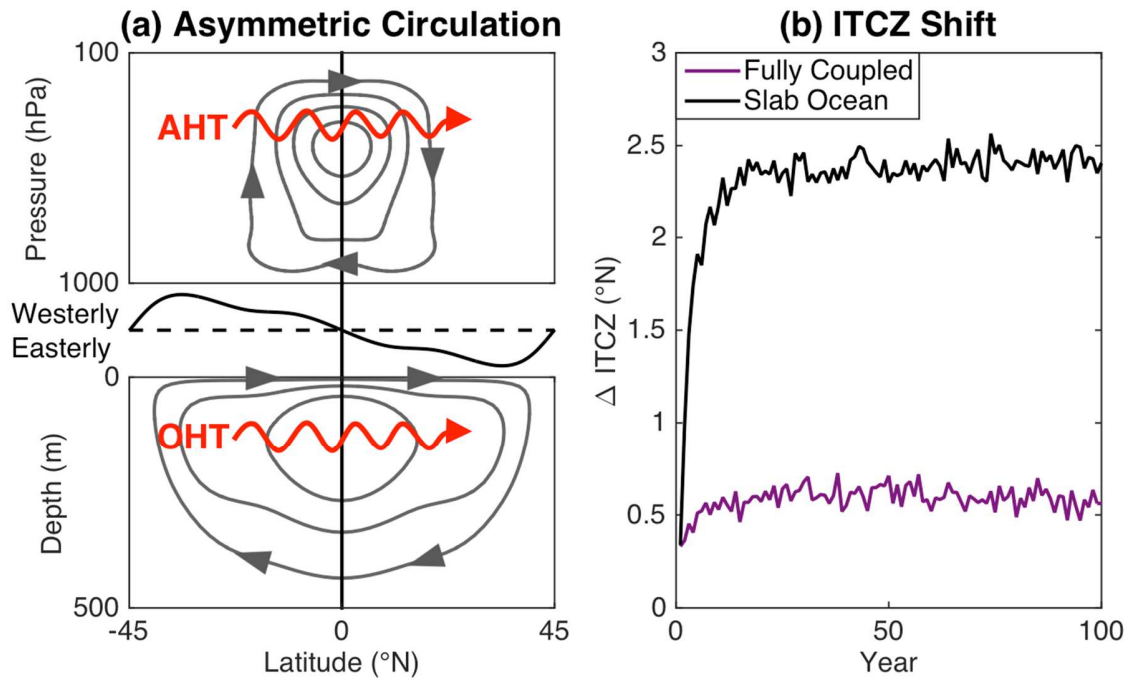


Figure 7. The tropical atmosphere and ocean response to NH cooling. **A.** Anomalies in zonal mean, annual mean atmospheric and shallow ocean circulation in response to NH cooling. Top panel shows anomalies in Hadley circulation; middle panel shows changes in zonal component of near-surface winds, showing strengthening of easterly winds in the NH and weakening in the SH; bottom panel shows resulting shallow ocean circulation anomalies. The anomalous atmospheric and ocean circulations both act to transport heat into the NH (red arrows). Contours indicate stream function anomalies. **B.** ITCZ shifts in response to cooling of one hemisphere in idealized climate model simulations. The black line shows a large ITCZ shift toward the warmer hemisphere in an uncoupled “slab” ocean simulation. The purple line shows a much smaller ITCZ shift in response to the same perturbation in a coupled simulation; the smaller response is primarily due to heat transport associated with the anomalous tropical ocean circulation shown in panel A. Note that the cooling perturbation and ITCZ responses in this simulation are not meant

to resemble those during a Heinrich stadial, only to demonstrate the role of the ocean in reducing
640 the likelihood of extreme ITCZ shifts. Adapted from Green and Marshall (2017).

response to ITCZ shifts further decreases the likelihood that the ITCZ was located far from the equator in past climates, as it increases the interhemispheric energy transport anomalies associated with ITCZ shifts.

645 Windblown dust provenance data from the Pacific Ocean tracing the latitudinal transition from sediment compositions similar to Asian dust (found north of the ITCZ today) to compositions similar to volcanic inputs and/or American dust (found south of the ITCZ today) have been interpreted as suggesting that the Pacific ITCZ was located at 30°N at 40 Ma and 12°N as recently as 8 Ma (Hyeong et al., 2005; Lyle et al., 2002; Pettke, 2002). As the position of the
650 Pacific ITCZ strongly influences the zonal-mean, annual-mean ITCZ position, these studies suggest either radically weaker heat transports associated with the Hadley cells and STCs in these warmer climates, very strong heating differences between the hemispheres, or the need for alternative interpretations of the dust provenance data. In particular, the northerly position of the dust provenance transition in the mid-Cenozoic may reflect low Asian dust inputs prior to the
655 Pliocene (An et al., 2001; Zhang et al., 2016) rather than a dramatic change in ITCZ location; reduced Asian dust flux and relatively constant inputs of volcanic ash and dust from sources in the Americas would be expected to lead to a stronger volcanic/American dust signature in subtropical Pacific sediments regardless of ITCZ changes.

Large changes in the Pacific ITCZ have also been suggested on more recent timescales.
660 Sachs et al. (2009) found evidence consistent with a 5° southward shift of the ITCZ in the central Pacific during the Little Ice Age (1400-1850 CE), and Jacobel et al. (2016) suggest that the central Pacific ITCZ shifted south by at least 4° during HS11 (~136-129 ka). If the magnitude of these shifts are taken to represent the zonal-mean ITCZ change during these events, they challenge the arguments put forward above and in McGee et al. (2014). However, both studies

665 are located in the region that shows the largest interannual variations in ITCZ-related
precipitation in the modern climate; as shown in Figure 2 in McGee et al. (2014), in the
observational record a 1° southward shift in the zonal mean precipitation centroid is
accompanied by a ~5° southward shift in the central Pacific precipitation centroid. Modern data
thus suggest that central Pacific ITCZ shifts indicated by these records may be much larger than
670 zonal-mean changes. In addition, the proxies used in these studies may track the precipitation
maximum associated with the ITCZ rather than the precipitation centroid metric used by
Donohoe et al. (2013) and McGee et al. (2014), and the precipitation maximum is susceptible to
larger jumps than the centroid.

675 **6. Conclusion and directions for future research**

Trade wind-sensitive proxies from Atlantic Ocean sites suggest that trade winds
intensified in the NH subtropics and weakened in the SH subtropics during millennial-scale NH
cooling events. Wind proxies in the Arabian Sea and eastern equatorial Pacific also indicate
intensification of NH trade winds during stadials. Angular momentum constraints and model
680 results indicate that these asymmetric trade wind changes are the expected response to cooling of
the NH relative to the SH, as a southward ITCZ shift is accompanied by an intensification of the
NH Hadley cell and associated trade winds, with an opposite response in the SH.

The coherent response of trade wind proxies during stadials demonstrates the potential of
trade wind-sensitive proxies to trace ITCZ shifts and Hadley cell changes. As shown in the maps
685 of Figure 2, trade wind anomalies have strong spatial coherence, particularly over the subtropical
oceans, making wind reconstructions highly representative of regional circulation changes.
Wind-based proxies may be particularly valuable in regions and time periods for which

precipitation proxies are scarce or difficult to interpret, but even in well-studied intervals they offer valuable independent insights into the tropical atmosphere's response to past climate changes.

This work suggests several important avenues for future research building upon the use of trade wind proxies to track ITCZ and Hadley cell changes. The lack of high-resolution, precisely dated trade wind proxy records in the southeastern Indian and southeastern Pacific Ocean presently limits our ability to trace trade wind responses to stadial events outside of the Atlantic basin, highlighting the need for additional records. Better documentation of trade wind changes in the Pacific basin is particularly important for shedding light on the magnitude of ITCZ shifts and STC changes during stadials. Trade wind proxies may also be useful in testing ITCZ shifts and Hadley cell dynamics in climates warmer than the present (e.g., the Pliocene or Cretaceous) (Hasegawa et al., 2012) or times in the Cenozoic when very large (10-25°) shifts of the ITCZ have been suggested based on dust provenance data (Lyle et al., 2002; Pettke, 2002). Modeling of upwelling and dust responses to wind variations may help constrain the trade wind changes necessary to explain proxy data and offer opportunities for quantitative data-model comparisons (Albani et al., 2016; Miller and Tziperman, 2017; Murphy et al., 2014).

Beyond tracing ITCZ shifts and Hadley cell strength, hemispherically asymmetric trade wind anomalies reconstructed here are expected to drive similarly asymmetric changes in the wind-driven ocean subtropical cells. This shallow ocean response to an ITCZ shift transports heat into the cooler hemisphere with a magnitude comparable to the anomalous atmospheric heat transport associated with the ITCZ shift itself; this amplifies heat transport anomalies associated with changes in the mean ITCZ position, thereby damping ITCZ variations induced by interhemispheric heating anomalies (Green and Marshall, 2017; Yang et al., 2017, 2013) and

reducing the likelihood of extreme ITCZ shifts. Understanding trade wind changes is thus essential not only to better constraining ITCZ shifts in past climates, but also to understanding the ocean and atmosphere dynamical changes that will determine the future response of the tropical circulation and precipitation to anthropogenic radiative forcing.

715

Acknowledgements

DM and LIB acknowledge support from NSF awards OCE-1030784 (DM) and OCE-1103262 (LIB), which funded the flux records from northwest African margin cores. JM, BG and EMC acknowledge support from NOAA award NA16OAR4310177. EDG acknowledges support from Compute Canada and the Canadian Foundation for Innovation. The authors would like to thank Jessica Tierney, one anonymous reviewer and editor Neil Roberts for comments that improved the manuscript.

720

References

- 725 Adkins, J., deMenocal, P., Eshel, G., 2006. The “African humid period” and the record of marine upwelling from excess ^{230}Th in Ocean Drilling Program Hole 658C. *Paleoceanography* 21, 1–14. doi:10.1029/2005PA001200
- Albani, S., Mahowald, N.M., Murphy, L.N., Raiswell, R., Moore, J.K., Anderson, R.F., McGee, D., Bradtmiller, L.I., Delmonte, B., Hesse, P.P., Mayewski, P.A., 2016. Paleodust variability since the Last Glacial Maximum and implications for iron inputs to the ocean. *Geophys. Res. Lett.* 3944–3954. doi:10.1002/2016GL067911
- 730 Alley, R.B., Meese, D.A., Shuman, C.A., Gow, A.J., Taylor, K.C., Grootes, P.M., White, J.W.C., Ram, M., Waddington, E.D., Mayewski, P.A., Zielinski, G.A., 1993. Abrupt increase in Greenland snow accumulation at the end of the Younger Dryas event. *Nature* 362, 527–529. doi:10.1038/362527a0
- 735 Altabet, M.A., Hoggins, M.J., Murray, D.W., 2002. The effect of millennial-scale changes in Arabian Sea denitrification on atmospheric CO_2 . *Nature* 415, 159–162. doi:10.1038/415159a
- Amrhein, D.E., Gebbie, G., Marchal, O., Wunsch, C., 2015. Inferring surface water equilibrium calcite $\delta\text{O}-18$ during the last deglacial period from benthic foraminiferal records: Implications for ocean circulation. *Paleoceanography* 30, 1470–1489. doi:10.1002/2014PA002743
- 740

- Amundson, R., Dietrich, W., Bellugi, D., Ewing, S., Nishiizumi, K., Chong, G., Owen, J., Finkel, R., Heimsath, A., Stewart, B., Caffee, M., 2012. Geomorphologic evidence for the late Pliocene onset of hyperaridity in the Atacama Desert. *Bull. Geol. Soc. Am.* 124, 1048–1070. doi:10.1130/B30445.1
- 745 An, Z., Kutzbach, J.E., Prell, W.L., Porter, S.C., 2001. Evolution of Asian monsoons and phased uplift of the Himalaya-Tibetan plateau since Late Miocene times. *Nature* 411, 62–66. doi:10.1038/35075035
- 750 Anderson, R.F., Cheng, H., Edwards, R.L., Fleisher, M.Q., Hayes, C.T., Huang, K.-F., Kadko, D., Lam, P.J., Landing, W.M., Lao, Y., 2016. How well can we quantify dust deposition to the ocean? *Phil. Trans. R. Soc. A* 374, 20150285. doi:10.1098/rsta.2015.0285
- Arbuszewski, J.A., deMenocal, P.B., Cléroux, C., Bradtmiller, L., Mix, A., 2013. Meridional shifts of the Atlantic intertropical convergence zone since the Last Glacial Maximum. *Nat. Geosci.* 6, 959–962. doi:10.1038/ngeo1961
- 755 Baker, P.A., 2001. The History of South American Tropical Precipitation for the Past 25,000 Years. *Science* 291, 640–643. doi:10.1126/science.291.5504.640
- Baker, P.A., Fritz, S.C., 2015. Nature and causes of Quaternary climate variation of tropical South America. *Quat. Sci. Rev.* 124, 31–47. doi:10.1016/j.quascirev.2015.06.011
- 760 Barbante, C., Barnola, J.-M., Becagli, S., Beer, J., Bigler, M., Boutron, C., Blunier, T., Castellano, E., Cattani, O., Chappellaz, J., Dahl-Jensen, D., Debret, M., Delmonte, B., Dick, D., Falourd, S., Faria, S., Federer, U., Fischer, H., Freitag, J., Frenzel, A., Fritzsche, D., Fundel, F., Gabrielli, P., Gaspari, V., Gersonde, R., Graf, W., Grigoriev, D., Hamann, I., Hansson, M., Hoffmann, G., Hutterli, M.A., Huybrechts, P., Isaksson, E., Johnsen, S.,
- 765 Jouzel, J., Kaczmarek, M., Karlin, T., Kaufmann, P., Kipfstuhl, S., Kohno, M., Lambert, F., Lambrecht, A., Lambrecht, A., Landais, A., Lawer, G., Leuenberger, M., Littot, G., Loulergue, L., Lüthi, D., Maggi, V., Marino, F., Masson-Delmotte, V., Meyer, H., Miller, H., Mulvaney, R., Narcisi, B., Oerlemans, J., Oerter, H., Parrenin, F., Petit, J.-R., Raisbeck, G., Raynaud, D., Röthlisberger, R., Ruth, U., Rybak, O., Severi, M., Schmitt, J., Schwander, J., Siegenthaler, U., Siggaard-Andersen, M.-L., Spahni, R., Steffensen, J.P., Stenni, B.,
- 770 Stocker, T.F., Tison, J.-L., Traversi, R., Udisti, R., Valero-Delgado, F., van den Broeke, M.R., van de Wal, R.S.W., Wagenbach, D., Wegner, A., Weiler, K., Wilhelms, F., Winther, J.-G., Wolff, E., 2006. One-to-one coupling of glacial climate variability in Greenland and Antarctica. *Nature* 444, 195–198. doi:10.1038/nature05301
- 775 Barker, S., Diz, P., Vautravers, M.J., Pike, J., Knorr, G., Hall, I.R., Broecker, W.S., 2009. Interhemispheric Atlantic seesaw response during the last deglaciation. *Nature* 457, 1097–1102. doi:10.1038/nature07770
- Blunier, T., Brook, E.J., 2001. Timing of millennial-scale climate change in Antarctica and Greenland during the last glacial period. *Science* 291, 109–112. doi:10.1126/science.291.5501.109
- 780 Blunier, T., Chappellaz, J., Schwander, J., Dallenbach, A., Stauffer, B., Stocker, T.F., Raynaud, D., Jouzel, J., Clausen, H.B., Hammer, C.U., Johnsen, S.J., 1998. Asynchrony of Antarctic and Greenland climate change during the last glacial period. *Nature* 394, 739–743. doi:10.1038/29447
- 785 Bond, G., Broecker, W., Johnsen, S., McManus, J., Labeyrie, L., Jouzel, J., Bonani, G., 1993. Correlations between climate records from North Atlantic sediments and Greenland ice. *Nature* 365, 143–147.
- Boyle, E.A., Keigwin, L., 1987. North Atlantic thermohaline circulation during the past 20,000

- years linked to high-latitude surface temperature. *Nature*. doi:10.1038/330035a0
- 790 Bradtmiller, L.I., McGee, D., Awalt, M., Evers, J., Yerxa, H., Kinsley, C.W., DeMenocal, P.B.,
2016. Changes in biological productivity along the northwest African margin over the past
20,000 years. *Paleoceanography* 31, 1–18. doi:10.1002/2015PA002862
- Broccoli, A.J., Dahl, K.A., Stouffer, R.J., 2006. Response of the ITCZ to Northern Hemisphere
cooling. *Geophys. Res. Lett.* 33, n/a-n/a. doi:10.1029/2005GL024546
- 795 Broecker, W.S., 1998. Paleocean circulation during the Last Deglaciation: A bipolar seesaw?
Paleoceanography 13, 119. doi:10.1029/97PA03707
- Broecker, W.S., Putnam, A.E., 2013. Hydrologic impacts of past shifts of Earth’s thermal
equator offer insight into those to be produced by fossil fuel CO₂. *Proc. Natl. Acad. Sci.*
110, 16710–16715. doi:10.1073/pnas.1301855110
- 800 Brown, N., Galbraith, E.D., 2016. Hosed vs. unhosed: Interruptions of the Atlantic Meridional
Overturning Circulation in a global coupled model, with and without freshwater forcing.
Clim. Past 12, 1663–1679. doi:10.5194/cp-12-1663-2016
- Buizert, C., Adrian, B., Ahn, J., Albert, M., Alley, R.B., Baggenstos, D., Bauska, T.K., Bay,
R.C., Bencivengo, B.B., Bentley, C.R., Brook, E.J., Chellman, N.J., Clow, G.D., Cole-Dai,
805 J., Conway, H., Cravens, E., Cuffey, K.M., Dunbar, N.W., Edwards, J.S., Fegyveresi, J.M.,
Ferris, D.G., Fitzpatrick, J.J., Fudge, T.J., Gibson, C.J., Gkinis, V., Goetz, J.J., Gregory, S.,
Hargreaves, G.M., Iverson, N., Johnson, J.A., Jones, T.R., Kalk, M.L., Kippenhan, M.J.,
Koffman, B.G., Kreutz, K., Kuhl, T.W., Lebar, D.A., Lee, J.E., Marcott, S.A., Markle, B.R.,
Maselli, O.J., McConnell, J.R., McGwire, K.C., Mitchell, L.E., Mortensen, N.B., Neff,
810 P.D., Nishiizumi, K., Nunn, R.M., Orsi, A.J., Pasteris, D.R., Pedro, J.B., Pettit, E.C., Buford
Price, P., Priscu, J.C., Rhodes, R.H., Rosen, J.L., Schauer, A.J., Schoenemann, S.W.,
Sendelbach, P.J., Severinghaus, J.P., Shturmakov, A.J., Sigl, M., Slawny, K.R., Souney,
J.M., Sowers, T.A., Spencer, M.K., Steig, E.J., Taylor, K.C., Twickler, M.S., Vaughn, B.H.,
Voigt, D.E., Waddington, E.D., Welten, K.C., Wendricks, A.W., White, J.W.C., Winstrup,
815 M., Wong, G.J., Woodruff, T.E., 2015. Precise inter-polar phasing of abrupt climate change
during the last ice age. *Nature* 520, 661–665. doi:10.1038/nature14401
- Cartapanis, O., Tachikawa, K., Bard, E., 2011. Northeastern Pacific oxygen minimum zone
variability over the past 70 kyr: Impact of biological production and oceanic ventilation.
Paleoceanography 26, 1–17. doi:10.1029/2011PA002126
- 820 Chelton, D., Freilich, M., Esbensen, S., 2000. Satellite observations of the wind jets off the
Pacific coast of Central America. Part I: Case studies and statistical characteristics. *Mon.*
Wea. Rev. 128, 1993–2018. doi:10.1175/1520-0493(2000)128<1993:SOOTWJ>2.0.CO;2
- Cheshire, H., Thurow, J., 2013. High-resolution migration history of the Subtropical High/Trade
Wind system of the northeastern Pacific during the last 55 years: Implications for glacial
825 atmospheric reorganization. *Paleoceanography* 28, 319–333. doi:10.1002/palo.20031
- Chiang, J.C.H., 2003. Sensitivity of the Atlantic Intertropical Convergence Zone to Last Glacial
Maximum boundary conditions. *Paleoceanography* 18, 1–18. doi:10.1029/2003PA000916
- Chiang, J.C.H., Bitz, C.M., 2005. Influence of high latitude ice cover on the marine Intertropical
Convergence Zone. *Clim. Dyn.* 25, 477–496. doi:10.1007/s00382-005-0040-5
- 830 Chiang, J.C.H., Friedman, A.R., 2012. Extratropical Cooling, Interhemispheric Thermal
Gradients, and Tropical Climate Change. *Annu. Rev. Earth Planet. Sci.* 40, 383–412.
doi:10.1146/annurev-earth-042711-105545
- Clement, A.C., Peterson, L.C., 2008. Mechanisms of Abrupt Climate Change of the Last Glacial
Period. *North* 46, 1–39. doi:10.1029/2006RG000204

- 835 Collins, J.A., Govin, A., Mulitza, S., Heslop, D., Zabel, M., Hartmann, J., Röhl, U., Wefer, G.,
2013. Abrupt shifts of the Sahara-Sahel boundary during Heinrich stadials. *Clim. Past* 9,
1181–1191. doi:10.5194/cp-9-1181-2013
- Dahl, K.A., Repeta, D.J., Goericke, R., 2004. Reconstructing the phytoplankton community of
the Cariaco Basin during the Younger Dryas cold event using chlorin steryl esters.
840 *Paleoceanography* 19, 1–13. doi:10.1029/2003PA000907
- Dahl, K., Broccoli, A., Stouffer, R., 2005. Assessing the role of North Atlantic freshwater
forcing in millennial scale climate variability: a tropical Atlantic perspective. *Clim. Dyn.*
24, 325–346. doi:10.1007/s00382-004-0499-5
- Dail, H., Wunsch, C., 2014. Dynamical Reconstruction of Upper-Ocean Conditions in the Last
845 Glacial Maximum Atlantic. *J. Clim.* 27, 807–823. doi:10.1175/JCLI-D-13-00211.1
- Dansgaard, W., Clausen, H.B., Gundestrup, N., Hammer, C.U., Johnsen, S.F., Kristinsdottir,
P.M., Reeh, N., 1982. A new Greenland deep ice core. *Science* 218, 1273–1277.
doi:10.1126/science.218.4579.1273
- Deplazes, G., Lückge, A., Peterson, L.C., Timmermann, A., Hamann, Y., Hughen, K.A., Röhl,
850 U., Laj, C., Cane, M.A., Sigman, D.M., Haug, G.H., 2013. Links between tropical rainfall
and North Atlantic climate during the last glacial period. *Nat. Geosci.* 6, 1–5.
doi:10.1038/ngeo1712
- Donohoe, A., Marshall, J., Ferreira, D., McGee, D., 2013. The Relationship between ITCZ
Location and Cross-Equatorial Atmospheric Heat Transport: From the Seasonal Cycle to
855 the Last Glacial Maximum. *J. Clim.* 26, 3597–3618. doi:10.1175/JCLI-D-12-00467.1
- Evans, M.N., Tolwinski-Ward, S.E., Thompson, D.M., Anchukaitis, K.J., 2013. Applications of
proxy system modeling in high resolution paleoclimatology. *Quat. Sci. Rev.* 76, 16–28.
doi:10.1016/j.quascirev.2013.05.024
- Farmer, E.C., deMenocal, P.B., Marchitto, T.M., 2005. Holocene and deglacial ocean
860 temperature variability in the Benguela upwelling region: Implications for low-latitude
atmospheric circulation. *Paleoceanography* 20, 1–16. doi:10.1029/2004PA001049
- Garcia, S.R., Kayano, M.T., 2010. Some evidence on the relationship between the South
American monsoon and the Atlantic ITCZ. *Theor. Appl. Climatol.* 99, 29–38.
doi:10.1007/s00704-009-0107-z
- 865 Gillette, D.A., 1974. On the production of soil wind erosion aerosols having the potential for
long range transport. *J. Rech. Atmos.* 8, 735–744.
- Goose, H., 2016. An additional step toward comprehensive paleoclimate reanalyses. *J. Adv.
Model. Earth Syst.* 8, 1501–1503. doi:doi:10.1002/2016MS000739
- Green, B., Marshall, J., 2017. Coupling of Trade Winds with Ocean Circulation Damps ITCZ
870 Shifts. *J. Clim.* JCLI-D-16-0818.1. doi:10.1175/JCLI-D-16-0818.1
- Grini, A., Zender, C.S., 2004. Roles of saltation, sandblasting, and wind speed variability on
mineral dust aerosol size distribution during the Puerto Rican Dust Experiment (PRIDE). *J.
Geophys. Res.* 109, 1–12. doi:10.1029/2003JD004233
- Harrison, S.P., Metcalfe, S.E., Street-Perrott, F.A., Pittock, A.B., Roberts, C.N., Salinger, M.J.,
875 1983. A climatic model of the Last Glacial/Interglacial transition based on
palaeotemperature and palaeohydrological evidence, in: Vogel, J.C. (Ed.), *Late Cainozoic
Palaeoclimates of the Southern Hemisphere*. Balkema, A.A., Rotterdam, Netherlands, pp.
21–34.
- 880 Hasegawa, H., Tada, R., Jiang, X., Suganuma, Y., Imsamut, S., Charusiri, P., Ichinnorov, N.,
Khand, Y., 2012. Drastic shrinking of the Hadley circulation during the mid-Cretaceous

- Supergreenhouse. *Clim. Past* 8, 1323–1337. doi:10.5194/cp-8-1323-2012
- Heaviside, C., Czaja, a., 2013. Deconstructing the Hadley cell heat transport. *Q. J. R. Meteorol. Soc.* 139, 2181–2189. doi:10.1002/qj.2085
- 885 Held, I.M., 2001. The Partitioning of the Poleward Energy Transport between the Tropical Ocean and Atmosphere. *J. Atmos. Sci.* 58, 943–948. doi:10.1175/1520-0469(2001)058<0943:TPOTPE>2.0.CO;2
- Hemming, S.R., 2004. Heinrich events: Massive late Pleistocene detritus layers of the North Atlantic and their global climate imprint. *Rev. Geophys.* 42. doi:10.1029/2003RG000128.1.INTRODUCTION
- 890 Henry, L.G., McManus, J.F., Curry, W.B., Roberts, N.L., Piotrowski, A.M., Keigwin, L.D., 2016. North Atlantic ocean circulation and abrupt climate change during the last glaciation. *Science* 352, 470–474. doi:10.1126/science.aaf5529
- Hodell, D.A., Anselmetti, F.S., Ariztegui, D., Brenner, M., Curtis, J.H., Gilli, A., Grzesik, D.A., Guilderson, T.J., Müller, A.D., Bush, M.B., 2008. An 85-ka record of climate change in 895 lowland Central America. *Quat. Sci. Rev.* 27, 1152–1165. doi:10.1016/j.quascirev.2008.02.008
- Hughen, K.A., Overpeck, J.T., Peterson, L.C., Trumbore, S., 1996. Rapid climate changes in the tropical Atlantic region during the last deglaciation. *Nature*. doi:10.1038/380051a0
- 900 Huguët, C., Kim, J.H., Damsté, J.S.S., Schouten, S., 2006. Reconstruction of sea surface temperature variations in the Arabian Sea over the last 23 kyr using organic proxies (TEX₈₆ and U_{37K'}). *Paleoceanography* 21, 1–13. doi:10.1029/2005PA001215
- Hyeong, K., Park, S.H., Yoo, C.M., Kim, K.H., 2005. Mineralogical and geochemical compositions of the eolian dust from the northeast equatorial Pacific and their implications on paleolocation of the Intertropical Convergence Zone. *Paleoceanography* 20, 1–11. 905 doi:10.1029/2004PA001053
- Ivanochko, T.S., Ganeshram, R.S., Brummer, G.J.A., Ganssen, G., Jung, S.J.A., Moreton, S.G., Kroon, D., 2005. Variations in tropical convection as an amplifier of global climate change at the millennial scale. *Earth Planet. Sci. Lett.* 235, 302–314. doi:10.1016/j.epsl.2005.04.002
- 910 Jacobel, A.W., McManus, J.F., Anderson, R.F., Winckler, G., 2016. Large deglacial shifts of the Pacific Intertropical Convergence Zone. *Nat. Commun.* 7, 10449. doi:10.1038/ncomms10449
- Kang, S.M., Held, I.M., Frierson, D.M.W., Zhao, M., 2008. The response of the ITCZ to extratropical thermal forcing: Idealized slab-ocean experiments with a GCM. *J. Clim.* 21, 915 3521–3532. doi:10.1175/2007JCLI2146.1
- Kienast, M., Kienast, S.S., Calvert, S.E., Eglinton, T.I., Mollenhauer, G., François, R., Mix, A.C., 2006. Eastern Pacific cooling and Atlantic overturning circulation during the last deglaciation. *Nature* 444, 512–512. doi:10.1038/nature05377
- 920 Kim, J.H., Schneider, R.R., Mulitza, S., Müller, P.J., 2003. Reconstruction of SE trade-wind intensity based on sea-surface temperature gradients in the Southeast Atlantic over the last 25 kyr. *Geophys. Res. Lett.* 30, 3–6. doi:10.1029/2003GL017557
- Kim, J.H., Schneider, R.R., Müller, P.J., Wefer, G., 2002. Interhemispheric comparison of deglacial sea-surface temperature patterns in Atlantic eastern boundary currents. *Earth Planet. Sci. Lett.* 194, 383–393. doi:10.1016/S0012-821X(01)00545-3
- 925 Klinger, B.A., Marotzke, J., 2000. Meridional heat transport by the subtropical cell. *J. Phys. Oceanogr.* 30, 696–705. doi:10.1175/1520-0485(2000)030<0696:MHTBTS>2.0.CO;2

- Lea, D.W., 2003. Synchronicity of Tropical and High-Latitude Atlantic Temperatures over the Last Glacial Termination. *Science* 301, 1361–1364. doi:10.1126/science.1088470
- 930 Le Mézo, P., Beaufort, L., Bopp, L., Braconnot, P., Kageyama, M., 2017. From monsoon to marine productivity in the Arabian Sea: Insights from glacial and interglacial climates. *Clim. Past* 13, 759–778. doi:10.5194/cp-13-759-2017
- Leduc, G., Vidal, L., Tachikawa, K., Bard, E., 2009. ITCZ rather than ENSO signature for abrupt climate changes across the tropical Pacific? *Quat. Res.* 72, 123–131. doi:10.1016/j.yqres.2009.03.006
- 935 Leech, P.J., Lynch-Stieglitz, J., Zhang, R., 2013. Western Pacific thermocline structure and the Pacific marine Intertropical Convergence Zone during the Last Glacial Maximum. *Earth Planet. Sci. Lett.* 363, 133–143. doi:10.1016/j.epsl.2012.12.026
- Li, C., Battisti, D.S., Schrag, D.P., Tziperman, E., 2005. Abrupt climate shifts in Greenland due to displacements of the sea ice edge 32, 2–5. doi:10.1029/2005GL023492
- 940 Little, M.G., Schneider, R.R., Kroon, D., Price, B., Summerhayes, C.P., Segl, M., 1997. Trade wind forcing of upwelling, seasonally, and Heinrich events as a response to sub-Milankovitch climate variability. *Paleoceanography* 12, 568–576. doi:10.1029/97PA00823
- Liu, Y., Chiang, J.C.H., Chou, C., Patricola, C.M., 2014. Atmospheric teleconnection mechanisms of extratropical North Atlantic SST influence on Sahel rainfall. *Clim. Dyn.* 1–15. doi:10.1007/s00382-014-2094-8
- 945 Liu, Z., Otto-Bliesner, B.L., He, F., Brady, E.C., Tomas, R., Clark, P.U., Carlson, A.E., Lynch-Stieglitz, J., Curry, W., Brook, E., Erickson, D., Jacob, R., Kutzbach, J., Cheng, J., 2009. Transient Simulation of Last Deglaciation with a New Mechanism for Bolling-Allerod Warming. *Science* 325, 310–314. doi:10.1126/science.1171041
- 950 Lyle, M., Wilson, P.A., Janacek, T.R., 2002. Leg 199 Summary, in: *Proceedings of the Ocean Drilling Program Initial Reports*. pp. 1–87.
- Mariotti, V., Bopp, L., Tagliabue, A., Kageyama, M., Swingedouw, D., 2012. Marine productivity response to Heinrich events: A model-data comparison. *Clim. Past* 8, 1581–1598. doi:10.5194/cp-8-1581-2012
- 955 Marshall, J., Donohoe, A., Ferreira, D., McGee, D., 2014. The ocean’s role in setting the mean position of the Inter-Tropical Convergence Zone. *Clim. Dyn.* 42, 1967–1979. doi:10.1007/s00382-013-1767-z
- McClymont, E.L., Ganeshram, R.S., Pichevin, L.E., Talbot, H.M., Van Dongen, B.E., Thunell, R.C., Haywood, A.M., Singarayer, J.S., Valdes, P.J., 2012. Sea-surface temperature records of Termination 1 in the Gulf of California: Challenges for seasonal and interannual analogues of tropical Pacific climate change. *Paleoceanography* 27, 1–15. doi:10.1029/2011PA002226
- 960 McCreary, Jr., J.P., Lu, P., 1994. Interaction between the Subtropical and Equatorial ocean circulations: The subtropical cell. *J. Phys. Oceanogr.* 24, 466–496.
- 965 McGee, D., Broecker, W.S., Winckler, G., 2010. Gustiness: The driver of glacial dustiness? *Quat. Sci. Rev.* 29, 2340–2350. doi:10.1016/j.quascirev.2010.06.009
- McGee, D., deMenocal, P.B., Winckler, G., Stuut, J.B.W., Bradtmiller, L.I., 2013. The magnitude, timing and abruptness of changes in North African dust deposition over the last 20,000 yr. *Earth Planet. Sci. Lett.* 371–372, 163–176. doi:10.1016/j.epsl.2013.03.054
- 970 McGee, D., Donohoe, A., Marshall, J., Ferreira, D., 2014. Changes in ITCZ location and cross-equatorial heat transport at the Last Glacial Maximum, Heinrich Stadial 1, and the mid-Holocene. *Earth Planet. Sci. Lett.* 390, 69–79. doi:10.1016/j.epsl.2013.12.043

- Miller, M.D., Tziperman, E., 2017. The effect of changes in surface winds and ocean stratification on coastal upwelling and sea surface temperatures in the Pliocene. *Paleoceanography*. doi:10.1002/2016PA002996
- 975
- Murphy, L.N., Clement, A.C., Albani, S., Mahowald, N.M., Swart, P., Arienzo, M.M., 2014. Simulated changes in atmospheric dust in response to a Heinrich stadial. *Paleoceanography* 29, 30–43. doi:10.1002/2013PA002550
- Neelin, J.D., Held, I.M., 1987. Modeling tropical convergence based on the moist static energy budget. *Mon. Weather Rev.* 115, 3–12.
- 980
- Ortiz, J.D., O’Connell, S.B., DeViscio, J., Dean, W., Carriquiry, J.D., Marchitto, T., Zheng, Y., van Geen, A., 2004. Enhanced marine productivity off western North America during warm climate intervals of the past 52 k.y. *Geology* 32, 521–524. doi:10.1130/G20234.1
- Oueslati, B., Bellon, G., 2015. The double ITCZ bias in CMIP5 models: interaction between SST, large-scale circulation and precipitation. *Clim. Dyn.* 44, 585–607. doi:10.1007/s00382-015-2468-6
- 985
- Peterson, L.C., 2000. Rapid Changes in the Hydrologic Cycle of the Tropical Atlantic During the Last Glacial. *Science* 290, 1947–1951. doi:10.1126/science.290.5498.1947
- Peterson, L.C., Overpeck, J.T., Kipp, N.G., Imbrie, J., 1991. A high-resolution Late Quaternary upwelling record from the anoxic Cariaco Basin, Venezuela. *Paleoceanography* 6, 99–119.
- 990
- Pettke, T., 2002. Cenozoic evolution of Asian climate and sources of Pacific seawater Pb and Nd derived from eolian dust of sediment core LL44-GPC3. *Paleoceanography* 17, 1–13. doi:10.1029/2001PA000673
- Placzek, C., Quade, J., Patchett, P.J., 2006. Geochronology and stratigraphy of late Pleistocene lake cycles on the southern Bolivian Altiplano: Implications for causes of tropical climate change. *Bull. Geol. Soc. Am.* 118, 515–532. doi:10.1130/B25770.1
- 995
- Pourmand, A., Marcantonio, F., Schulz, H., 2004. Variations in productivity and eolian fluxes in the northeastern Arabian Sea during the past 110 ka. *Earth Planet. Sci. Lett.* 221, 39–54. doi:10.1016/S0012-821X(04)00109-8
- 1000
- Prange, M., Steph, S., Schulz, M., Keigwin, L.D., 2010. Inferring moisture transport across Central America: Can modern analogs of climate variability help reconcile paleosalinity records? *Quat. Sci. Rev.* 29, 1317–1321. doi:10.1016/j.quascirev.2010.02.029
- Rea, D.K., 1994. The paleoclimatic record provided by eolian deposition in the deep sea: The geologic history of wind. *Rev. Geophys.* 32, 159–195.
- 1005
- Romero, O.E., Kim, J.H., Donner, B., 2008. Submillennial-to-millennial variability of diatom production off Mauritania, NW Africa, during the last glacial cycle. *Paleoceanography* 23, PA3218. doi:10.1029/2008PA001601
- Romero, O.E., Leduc, G., Vidal, L., Fischer, G., 2011. Millennial variability and long-term changes of the diatom production in the eastern equatorial Pacific during the last glacial cycle. *Paleoceanography* 26, 1–11. doi:10.1029/2010PA002099
- 1010
- Roskin, J., Tsoar, H., Porat, N., Blumberg, D.G., 2011. Palaeoclimate interpretations of Late Pleistocene vegetated linear dune mobilization episodes: Evidence from the northwestern Negev dunefield, Israel. *Quat. Sci. Rev.* 30, 3364–3380. doi:10.1016/j.quascirev.2011.08.014
- 1015
- Sachs, J.P., Sachse, D., Smittenberg, R.H., Zhang, Z., Battisti, D.S., Golubic, S., 2009. Southward movement of the Pacific intertropical convergence zone AD 1400–1850. *Nat. Geosci.* 2, 519–525. doi:10.1038/ngeo554
- Sarnthein, M., Tetzlaff, G., Koopmann, B., Wolter, K., Pflaumann, U., 1981. Glacial and

- interglacial wind regimes over the eastern subtropical Atlantic and North-West Africa.
1020 Nature 293, 193–196. doi:10.1038/293193a0
- Saukel, C., 2011. Tropical Southeast Pacific continent-ocean-atmosphere linkages since the
Pliocene inferred from eolian dust. University of Bremen.
- Saukel, C., Lamy, F., Stuut, J.B.W., Tiedemann, R., Vogt, C., 2011. Distribution and provenance
of wind-blown SE Pacific surface sediments. *Mar. Geol.* 280, 130–142.
1025 doi:10.1016/j.margeo.2010.12.006
- Schmittner, A., Galbraith, E.D., Hostetler, S.W., Pedersen, T.F., Zhang, R., 2007. Large
fluctuations of dissolved oxygen in the Indian and Pacific oceans during Dansgaard-
Oeschger oscillations caused by variations of North Atlantic Deep Water subduction.
Paleoceanography 22, 1–17. doi:10.1029/2006PA001384
- 1030 Schneider, T., Bischoff, T., Haug, G.H., 2014. Migrations and dynamics of the intertropical
convergence zone. *Nature* 513, 45–53. doi:10.1038/nature13636
- Schulz, H., van Rad, U., Erlenkeuser, H., 1998. Correlation between Arabian Sea and Greenland
climate oscillations of the past 110,000 years. *Nature* 393, 54–57. doi:10.1038/31750
- Shakun, J.D., Clark, P.U., He, F., Marcott, S.A., Mix, A.C., Liu, Z., Otto-Bliesner, B.,
1035 Schmittner, A., Bard, E., 2012. Global warming preceded by increasing carbon dioxide
concentrations during the last deglaciation. *Nature* 484, 49–54. doi:10.1038/nature10915
- Stager, J.C., Ryves, D.B., Chase, B.M., Pausata, F.S.R., 2011. Catastrophic Drought in the Afro-
Asian Monsoon Region During Heinrich Event 1. *Science* 331, 1299–1302.
doi:10.1126/science.1198322
- 1040 Stríkis, N.M., Chiessi, C.M., Cruz, F.W., Vuille, M., Cheng, H., de Souza Barreto, E.A.,
Mollenhauer, G., Kasten, S., Karmann, I., Edwards, R.L., Bernal, J.P., Sales, H. dos R.,
2015. Timing and structure of Mega-SACZ events during Heinrich Stadial 1. *Geophys. Res.
Lett.* 42, 5477–5484. doi:10.1002/2015GL064048
- Stuut, J.B.W., Prins, M.A., Schneider, R.R., Weltje, G.J., Fred Jansen, J.H., Postma, G., 2002. A
1045 300-kyr record of aridity and wind strength in southwestern Africa: Inferences from grain-
size distributions of sediments on Walvis Ridge, SE Atlantic. *Mar. Geol.* 180, 221–233.
doi:10.1016/S0025-3227(01)00215-8
- Stuut, J.B.W., Temmesfeld, F., De Deckker, P., 2014. A 550ka record of aeolian activity near
North West Cape, Australia: Inferences from grain-size distributions and bulk chemistry of
1050 SE Indian Ocean deep-sea sediments. *Quat. Sci. Rev.* 83, 83–94.
doi:10.1016/j.quascirev.2013.11.003
- Takesue, R.K., van Geen, A., Carriquiry, J.D., Ortiz, E., Godinez-Orta, L., Granados, I.,
Saldivar, M., Ortlieb, L., Escribano, R., Guzman, N., Castilla, J.C., Varas, M., Salamanca,
M., Figueroa, C., 2004. Influence of coastal upwelling and El Niño-Southern Oscillation on
1055 nearshore water along Baja California and Chile: Shore-based monitoring during 1997-
2000. *J. Geophys. Res.* 109. doi:10.1029/2003JC001856
- Taylor, K.C., Lamorey, G.W., Doyle, G.A., Alley, R.B., Grootes, P.M., Mayewski, P. a., White,
J.W.C., Barlow, L.K., 1993. The “flickering switch” of late Pleistocene climate change.
Nature 361, 432–436. doi:10.1038/361432a0
- 1060 Tierney, J.E., Pausata, F.S.R., deMenocal, P., 2015. Deglacial Indian monsoon failure and North
Atlantic stadials linked by Indian Ocean surface cooling. *Nat. Geosci.* 9, 46–50.
doi:10.1038/ngeo2603
- Timmermann, A., Krebs, U., Justino, F., Goosse, H., Ivanochko, T., 2005. Mechanisms for
millennial-scale global synchronization during the last glacial period. *Paleoceanography* 20.

- 1065 doi:10.1029/2004PA001090
Tjallingii, R., Claussen, M., Stuut, J.-B.W., Fohlmeister, J., Jahn, A., Bickert, T., Lamy, F., Röhl, U., 2008. Coherent high- and low-latitude control of the northwest African hydrological balance. *Nat. Geosci.* 1, 670–675. doi:10.1038/ngeo289
- Trenberth, K.E., Caron, J.M., 2001. Estimates of Meridional Atmosphere and Ocean Heat
1070 Transports. *J. Clim.* 14, 3433–3443. doi:10.1175/1520-0442(2001)014<3433:EOMAAO>2.0.CO;2
- Tsoar, H., 2005. Sand dunes mobility and stability in relation to climate. *Phys. A Stat. Mech. its Appl.* 357, 50–56. doi:10.1016/j.physa.2005.05.067
- Vellinga, M., Wood, R.A., 2002. Global climatic impacts of a collapse of the Atlantic
1075 thermohaline circulation. *Clim. Change* 54, 251–267. doi:10.1023/A:1016168827653
- Vuille, M., Burns, S.J., Taylor, B.L., Cruz, F.W., Bird, B.W., Abbott, M.B., Kanner, L.C., Cheng, H., Novello, V.F., 2012. A review of the South American monsoon history as recorded in stable isotopic proxies over the past two millennia. *Clim. Past* 8, 1309–1321. doi:10.5194/cp-8-1309-2012
- 1080 Wang, W., Evan, A., Flamant, C., Lavaysse, C., 2015. On the Decadal Scale Correlation between African Dust and Sahel Rainfall: the Role of Saharan Heat Low-Forced Winds. *Sci. Adv.* 1, e1500646.
- Wang, X., Auler, A.S., Edwards, R.L., Cheng, H., Cristalli, P.S., Smart, P.L., Richards, D.A., Shen, C.-C., 2004. Wet periods in northeastern Brazil over the past 210 kyr linked to distant
1085 climate anomalies. *Nature* 432, 740–743. doi:10.1038/nature03067
- Wang, X., Auler, A.S., Edwards, R.L., Cheng, H., Ito, E., Wang, Y., Kong, X., Solheid, M., 2007. Millennial-scale precipitation changes in southern Brazil over the past 90,000 years. *Geophys. Res. Lett.* 34, n/a-n/a. doi:10.1029/2007GL031149
- Wang, X., Edwards, R.L., Auler, A.S., Cheng, H., Kong, X., Wang, Y., Cruz, F.W., Dorale, J.A.,
1090 Chiang, H.-W., 2017. Hydroclimate changes across the Amazon lowlands over the past 45,000 years. *Nature* 541, 204–207. doi:10.1038/nature20787
- Wang, Y.J., 2001. A High-Resolution Absolute-Dated Late Pleistocene Monsoon Record from Hulu Cave, China. *Science* 294, 2345–2348. doi:10.1126/science.1064618
- Yang, H., Wang, Y., Liu, Z., 2013. A modelling study of the Bjerknes compensation in the
1095 meridional heat transport in a freshening ocean. *Tellus A* 65, 18480. doi:10.3402/tellusa.v65i0.18480
- Yang, H., Wen, Q., Yao, J., Wang, Y., 2017. Bjerknes Compensation in Meridional Heat Transport under Freshwater Forcing and the Role of Climate Feedback. *J. Clim.* 30, 5167–5185. doi:10.1175/JCLI-D-16-0824.1
- 1100 Zhang, R., Delworth, T.L., 2005. Simulated tropical response to a substantial weakening of the Atlantic thermohaline circulation. *J. Clim.* 18, 1853–1860. doi:10.1175/JCLI3460.1
- Zhang, W., Chen, J., Ji, J., Li, G., 2016. Evolving flux of Asian dust in the North Pacific Ocean since the late Oligocene. *Aeolian Res.* 23, 1–11. doi:10.1016/j.aeolia.2016.09.004

Table 1. Core sites discussed in text.

Region	Core	Lat. (°N)	Long. (°E)	# wind proxies	Stadial trade wind change (+/-)	Confidence (1=high; 0=low)	Type(s) of proxies	References
S Atlantic	MD96-2094	-20.00	9.26	1	-	1	Dust grain size	Stuut et al., 2002
	GeoB1711-4	-23.32	12.38	1	-	1	Upwelling-associated foram species	Little et al., 1997
S Indian	MD00-2361	-22.08	113.48	1	-	0	Dust abundance	Stuut et al., 2015
S Pacific	ODP1237	-17.60	-76.38	1	-	0	Dust flux	Saukel, 2011
NE Atlantic	OCE437-7 GC68	19.36	-17.28	3	+	1	Dust, opal, organic C fluxes	McGee et al., 2013; Bradtmitter et al., 2016
	OCE437-7 GC49	23.21	-17.85	3	+	1	Dust, opal, organic C fluxes	McGee et al., 2013; Bradtmitter et al., 2016
	OCE437-7 GC37	26.82	-15.12	3	+	1	Dust, opal, organic C fluxes	McGee et al., 2013; Bradtmitter et al., 2016
	ODP 658	20.75	-18.58	3	+	1	Dust flux, opal flux, SST	Adkins et al., 2006; Zhao et al., 1995
	GeoB7926-2	20.22	-18.45	2	+	1	Opal/diatom abundance, SST	Romero et al., 2008
NW Atlantic	PL07-39PC/ MD03- 2621	10.70	-64.94	2	+	1	SST, sediment color, upwelling species abundance	Lea et al., 2003, Deplazes et al., 2013
NE Pacific	ME0005A-24JC	0.02	-86.46	2	+	0	SST, organic C flux	Kienast et al., 2006
	MD02-2529	8.21	-84.12	1	+	1	Opal/diatom abundance	Romero et al., 2011
Arabian Sea	SO90-111KL	23.10	66.48	1	+	1	Organic C abundance	Schulz et al., 1998
	SO90-136KL	23.12	66.50	1	+	1	Organic C abundance	Schulz et al., 1998
	RC27-14	18.25	57.66	1	+	1	N isotopes	Altabet et al., 2002
	RC27-23	17.99	57.59	1	+	1	N isotopes	Altabet et al., 2002
	NIOP905	10.77	51.95	3	+	1	Org. C abundance, N isotopes, subsurface temperature	Ivanochko et al., 2005; Huguet et al., 2006
	P178-15P	11.96	44.30	1	+	1	Subsurface temperature	Tierney et al., 2015
	74KL	14.32	57.33	1	+	1	Subsurface temperature	Huguet et al., 2006
93KL	23.58	64.22	2	+	1	Dust flux, authigenic uranium	Pourmand et al., 2004	